Contents lists available at ScienceDirect

European Journal of Medicinal Chemistry

journal homepage: http://ees.elsevier.com

Research paper

Structural features and functional activities of benzimidazoles as NOD2 antagonists

Samo Guzelj [a], Martina Gobec [a], Dunja Urbančič [a], Irena Mlinarič-Raščan [a], Emanuela Corsini [b], Žiga Jakopin [a,*]

[a] Faculty of Pharmacy, University of Ljubljana, Aškerčeva 7, 1000, Ljubljana, Slovenia
[b] Laboratory of Toxicology, Department of Environmental Science and Policy, University of Milan, Via Balzaretti 9, 20133, Milan, Italy

ARTICLE INFO

Article history:
Received 19 November 2019
Accepted 20 January 2020
Available online xxx

Keywords
NOD2 antagonist
NOD1 antagonist
NF-κB activation
Immunomodulation
Interleukin-8
Tumor necrosis factor-α

ABSTRACT

NOD1 and NOD2 are pattern recognition receptors that have important roles in innate immune responses. Although their overactivation has been linked to a number of diseases, NOD2 in particular remains a virtually unexploited target in this respect, with only one structural class of inhibitor reported. To gain insight into the structure-activity relationships of NOD2 antagonists, a series of novel analogs was designed and synthesized, and then screened for antagonist activity *versus* NOD2, and counter-screened *versus* NOD1. Compounds **32** and **38** were identified as potent and moderately selective NOD2 antagonists, and **33** and **42** as dual NOD1/NOD2 antagonists, with balanced activities against both targets in the low micromolar range. These data enable in-depth exploration of their structure-activity relationships and provide deeper understanding of the structural features required for NOD2 antagonism.

1. Introduction

The intracellular nucleotide-binding oligomerization domain (NOD)-like receptors include NOD1 and NOD2, and they are important in the generation of innate immune responses through their recognition of distinct pathogen-associated molecular patterns [1–3]. NOD1 and NOD2 have distinct expression profiles in cells and tissues throughout the body: NOD1 is extensively expressed in a variety of cell types and has a wide tissue distribution, while NOD2 is predominantly expressed in professional immune cells and various epithelial cells [4]. Activation of NOD1 and NOD2 by their cognate ligands D-glutamyl-meso-diaminopimelic acid (iE-DAP) [5–7] and muramyl dipeptide (MDP) [8,9], respectively, activates their downstream signaling pathways, which include, in turn, nuclear factor κB (NF-κB) and mitogen-associated protein kinases, to promote inflammatory responses [1,3].

Overactivation of the NOD-like receptors is the underlying cause of a number of diseases, including inflammatory disorders, autoimmune diseases, and certain types of cancers [4,10–12]. Regulated suppression of NOD activity has thus been highlighted as a novel approach in the treatment of these diseases, while keeping other innate immune mechanisms intact [10,11,13]. Furthermore, NOD antagonists have demonstrated unique antitumor activities through the prevention of the formation of the inflammatory tumor microenvironment [4,14].

However, only a handful of NOD antagonists have been developed thus far (Fig. 1). Indeed, although several classes of NOD1-selective antagonists are already known, such as noditinib-1 (**ML130**) [15–19], for NOD2, the benzimidazole diamides, which are exemplified by **GSK669**, represent the only reported class of NOD2-selective antagonists identified to date [20]. NOD2-selective antagonists are thus urgently needed as chemical probes to allow for further definition of the role of NOD2 in inflammatory processes. In addition, dual NOD1/2 antagonists with balanced inhibition of both of these targets have been reported (e.g., Fig. 1, **SZA-39**) [4,21].

We have been engaged in the development of NOD ligands, as both agonists and antagonists [21–28], and here we report on a novel series of NOD antagonists. We made use of the existing knowledge of the structure-activity relationships (SARs) of the only NOD2-selective antagonists reported to date, to design and synthesize new compounds based on the benzimidazole scaffold of **GSK669**. Indeed, the mechanism of action and the binding site of **GSK669** have yet to be defined, due to difficulties in the expression and purification of the functional full-length NOD2 protein [29]. However, **GSK669** is known not to inhibit receptor-interacting serine-threonine protein kinase 2 and not to interfere with uptake of MDP [20]. This implies that the NOD2-antagonist activity of **GSK669** can be ascribed to its direct action on NOD2.

Reporter-gene assays in NOD1-and NOD2-overexpressing human embryonic kidney (HEK)-Blue cell lines were then used to screen

Abbreviations: AcOH, acetic acid; Boc, tert-butoxycarbonyl; C12-iE-DAP, lauroyl-γ-D-glutamyl-*meso*-diaminopimelic acid; EDC, 1-ethyl-3-(3-dimethylaminopropyl)carbodiimide; HEK, human embryonic kidney; HOBt, hydroxybenzotriazole; iE-DAP, γ-D-glutamyl-*meso*-diaminopimelic acid; IL, interleukin; LPS, lipopolysaccharide; MDP, muramyl dipeptide; NF-κB, nuclear factor κB; NOD, nucleotide-binding oligomerization domain protein; PBMCs, peripheral blood mononuclear cells; SAR, structure-activity relationship; TBAI, tetrabutylammonium iodide; TNF-α, tumor necrosis factor-α.

* Corresponding author.
E-mail address: ziga.jakopin@ffa.uni-lj.si (Ž. Jakopin)

https://doi.org/10.1016/j.ejmech.2020.112089
0223-5234/

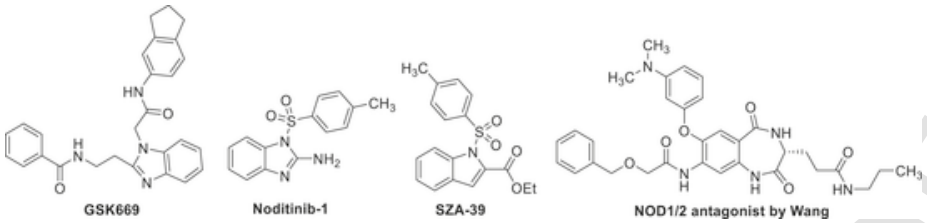

Fig. 1. Representative NOD2 (GSK669) and NOD1 (noditinib-1) antagonists, and dual NOD1/NOD2 antagonists (SZA-39, Wang).

these synthesized compounds, initially focusing on NOD2-antagonist activity, with counter-screening for NOD1-antagonist activity, as described previously [21,30]. The selected compounds were then investigated in terms of inhibition of NOD-agonist-induced interleukin (IL)-8 production from human leukemia monocytic THP-1 cells [31]. They were then additionally examined for their suppression of tumor necrosis factor (TNF)-α release from doubly stimulated (NOD agonist plus lipopolysaccharide [LPS]) THP-1 cells [31]. Finally, the effects of the best of these novel NOD antagonists was tested on cytokine release from human primary peripheral blood mononuclear cells (PBMCs).

2. Results

2.1. Design

The recently reported NOD2-selective antagonist **GSK669** [20] was chosen as the starting point for the design of the novel antagonists in this study. As no information regarding the binding mode of **GSK669** was available, the design here relied on a traditional SAR-based approach. We designed a small focused library of **GSK669** analogs with a benzimidazole central core. A previously reported SAR analysis of the benzimidazole series implicated inclusion of 5-aminoindane and an unsubstituted benzimidazole phenyl ring as optimal for NOD2-antagonist activity [20]: therefore, these were kept intact. Instead, other functionalities were varied to enter unexplored regions of the chemical space and to provide novel optimization opportunities.

Using a ligand-based design, we investigated the effects of the following structural changes (see Fig. 2): (*i*) replacement of the side-chain phenyl ring with its surrogates (Fig. 2, blue); (*ii*) variation of the length of the spacer (Fig. 2, green); and (*iii*) introduction of bioisosteres of the amide linkage that connects the phenyl and benzimidazole moieties (Fig. 2, red). The main objective of the present study was to identify small-molecule NOD2 antagonists through ligand-based optimization of this known NOD2 antagonist.

2.2. Chemistry

Initially, homologs were prepared of reference compound **GSK669** that incorporated spacers of different lengths that spanned the benzimidazole and the phenyl group, as depicted in Scheme 1. First, 1,2-diaminobenzene was coupled with the commercially available tert-butoxycarbonyl (Boc)-protected amino acids, using standard 1-ethyl-3-(3-dimethylaminopropyl)carbodiimide (EDC)/hydroxybenzotriazole (HOBt) coupling to derive the *N*-acylated 1,2-diaminobenzene derivatives **1**–**3**. These crude products underwent thermal cyclization in refluxing acetic acid (AcOH) to derive benzimidazoles **4**–**6** [20]. Treatment of benzimidazoles **4**–**6** with ethyl 2-bromoacetate in the presence of K_2CO_3 and tetrabutylammonium iodide (TBAI) in acetonitrile resulted in alkylation of the benzimidazole ring nitrogen, and yielded the *N*-alkylated analogs **7**–**9**. Next, acidolytic removal of the *N*-Boc protecting group was achieved by reacting these with 4 M HCl/AcOH. The *N*-deprotected amines were immediately reacted with benzoyl chloride, to derive their *N*-benzoylated analogs **10**–**12**. In the final step, these were first converted to free acids by alkaline hydrolysis of the ethyl ester moieties, and then they were coupled with 5-aminoindane, to yield the products **13**–**15**. The retroamide analog of **13** was prepared in a similar manner, by coupling 1,2-diaminobenzene with 4-oxo-4-(phenylamino)butanoic acid, to derive compound **16**, which was converted into the benzimidazole **17** by thermal cyclization. Alkylation of **17** with ethyl 2-bromoacetate produced compound **18**, which was hydrolyzed and coupled with 5-aminoindane to derive the retroamide **19**.

Next, we generated several compounds with diverse functionalities to determine how replacements of the phenyl moiety and/or the amide linkage affect the NOD2-antagonist activity of **GSK669**. Representative *N*-benzylated, *N*-benzoylated, and *N*-sulfonylated derivatives were therefore synthesized (Scheme 2). The starting key intermediate **8** was first *N*-deprotected by treatment with 4 M HCl/AcOH, to derive the free amine, which was reacted with the corresponding acyl/sulfonyl chlorides to give the *N*-substituted products **20**–**26**. These raw products were converted into their free acids by alkaline hydrolysis, and

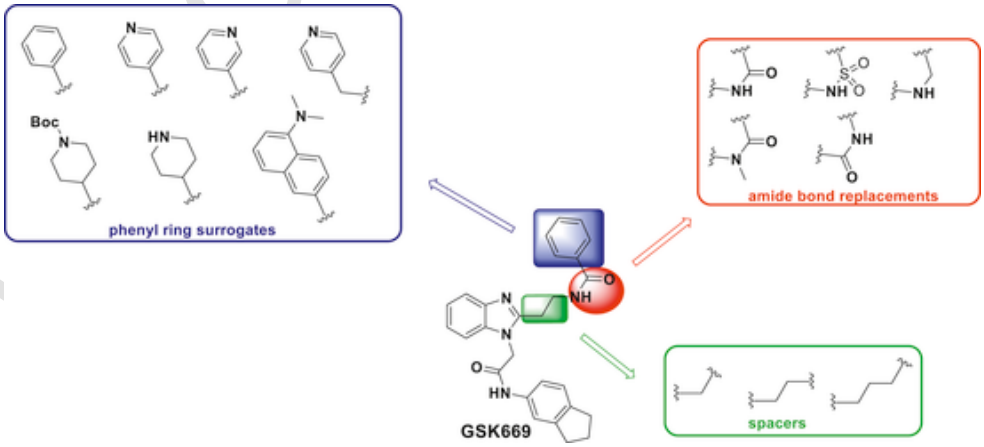

Fig. 2. Design of the NOD2 antagonists through structural modifications of the lead **GSK669**.

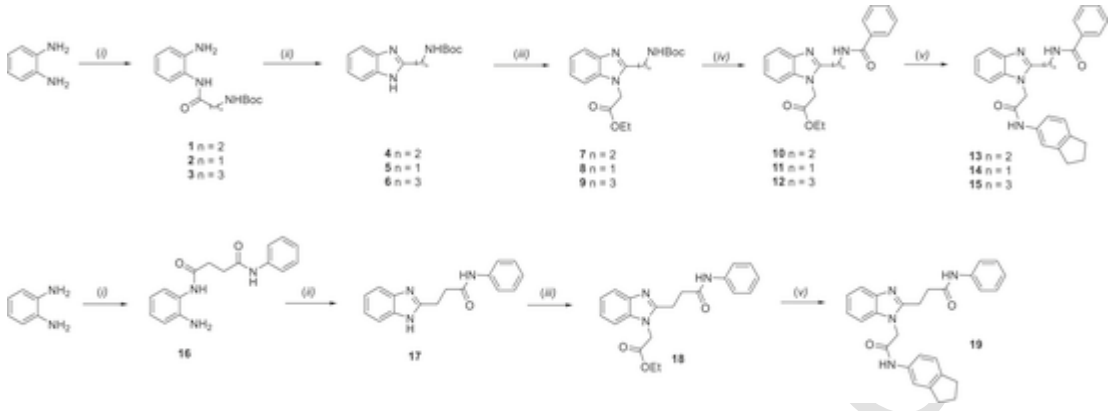

Scheme 1. Synthesis of the **GSK669** homologs. Reagents and conditions: (*i*) $BocNH(CH_2)_nCOOH$ or 4-oxo-4-(phenylamino)butanoic acid, EDC, HOBt, DIPEA, DMAP, THF; (*ii*) AcOH, 80 °C; (*iii*) ethyl 2-bromoacetate, K_2CO_3, TBAI, acetonitrile, 60 °C; (*iv*) 4 M HCl/AcOH, then benzoyl chloride, Et_3N, THF; (*v*) 1 M NaOH, THF then 5-aminoindane, EDC, HOBt, DIPEA, DMF.

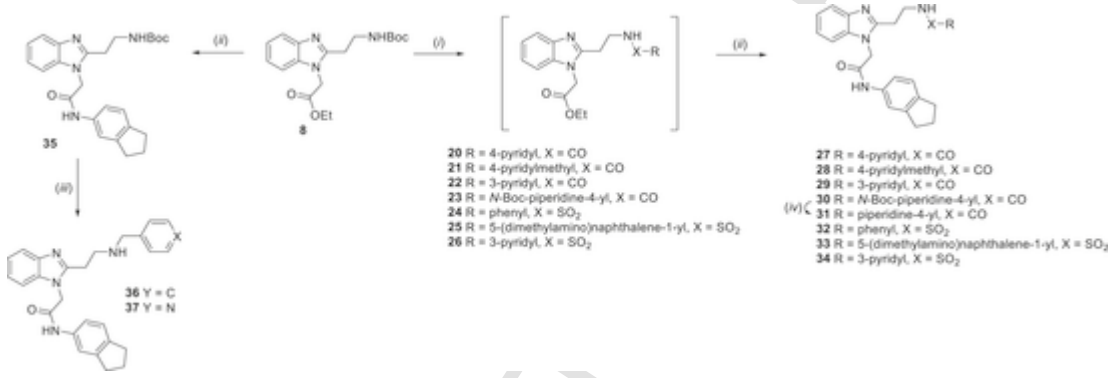

Scheme 2. Synthesis of *N*-benzylated, *N*-benzoylated, and *N*-sulfonylated derivatives of **GSK669**. Reagents and conditions: (*i*) 4 M HCl/AcOH, then the corresponding acyl/sulfonyl chloride, Et_3N, THF; (*ii*) 1 M NaOH, THF then 5-aminoindane, EDC, HOBt, DIPEA, DMF; (*iii*) 4 M HCl/AcOH, then benzaldehyde or 4-pyridine-carboxaldehyde, $Na(AcO)_3BH$, AcOH, 1,2-dichloroethane; (*iv*) 4 M HCl/AcOH.

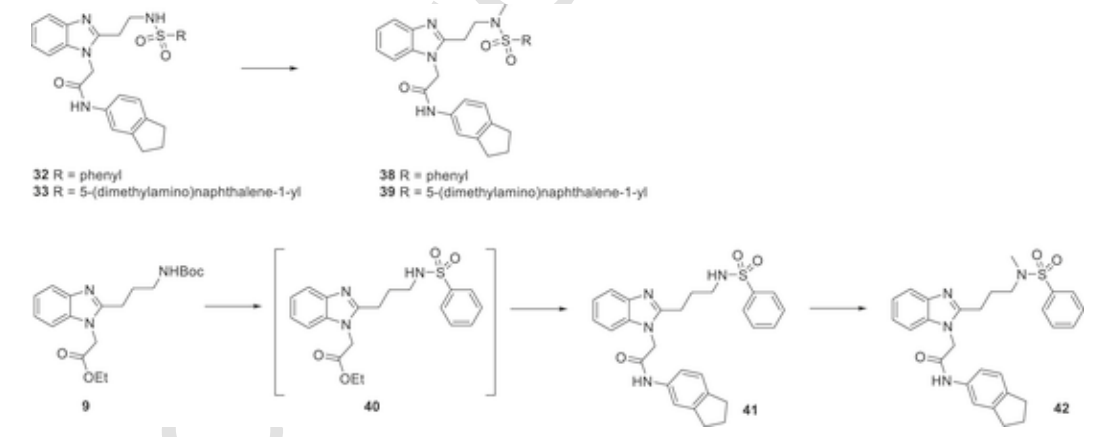

Scheme 3. Synthesis of the methylated derivatives of **GSK669**. Reagents and conditions: (*i*) 2-methyl iodide, K_2CO_3, TBAI, acetonitrile, 60 °C; (*ii*) 4 M HCl/AcOH, then the corresponding sulfonyl chloride, Et_3N, THF; (*iii*) 1 M NaOH, THF then 5-aminoindane, EDC, HOBt, DIPEA, DMF.

were immediately coupled with 5-aminoindane, to derive products **27**–**30** and **32**–**34**. Compound **31** was obtained by an additional step, by reacting **30** with 4 M HCl/AcOH .

Alternatively, to obtain the *N*-alkylated analogs **36** and **37**, the starting key intermediate **8** was first hydrolyzed to its free acid, and then reacted with 5-aminoindane under standard EDC-coupling conditions, to derive compound **35**. In the final step, acidolytic removal of the *N*-Boc protecting group was achieved by treating **35** with 4 M HCl/AcOH, to derive the free amine, which underwent reductive amination with the corresponding aldehyde, to yield the reduced amide isosteres **36** and **37** [32,33].

Finally, based on the information that methylation of the nitrogen adjacent to the phenyl moiety in **GSK669** promoted significant increase in its activity, methylated analogs were prepared for the best compounds in this series (see Scheme 3). Sulfonamides **32** and **33** were converted to their *N*-methylated counterparts **38** and **39** by treatment with methyl iodide in the presence of K_2CO_3 and TBAI in acetonitrile, which achieved selective methylation of the sulfonamide nitrogen.

In addition, examination of the SARs of the first series of compounds revealed that a spacer length of three methylene units and replacement of the amide linkage by its sulfonamide counterpart increased the selectivity of these compounds towards NOD2. Therefore, an analog that combined both of these structural features was synthesized using a well-established procedure. The *N*-Boc protecting group of **9** was acidolytically removed, and the resulting free amine was immediately reacted with benzenesulfonyl chloride, to derive **40**. This was then hydrolyzed and coupled with 5-aminoindane, yielding product **41**. This last was also converted to its *N*-methylated counterpart **42** by treatment with methyl iodide.

2.3. Biological characterization

2.3.1. Cytotoxicities of the synthesized compounds

The 3-(4,5-dimethylthiazol-2-yl)-5-(3-carboxymethoxyphenyl)-2-(4-sulfophenyl)-2H-tetrazolium (MTS) cell viability assay was used first to determine the proliferation rates of the HEK-Blue NOD2 and HEK-Blue NOD1 cells in the presence of reference NOD2 and NOD1 antagonists and of the synthesized potential NOD antagonists, to screen these compounds for cytotoxicity. The cells were treated for 18 h with each compound of interest at concentrations of up to 20 μM. Comparison of the resulting metabolic activities with that of the untreated control showed that almost all of these compounds (except for compound **36**) were well tolerated by the HEK-Blue NOD2 and/or NOD1 cells, as their residual metabolic activities did not fall below 80% of the control at the highest concentrations tested (Fig. 3).

2.3.2. NOD-antagonist activities of the synthesized compounds

These potential NOD2 antagonists were initially examined here for their antagonist activities using the HEK-Blue assay. The HEK-Blue NOD2 cells stably overexpressed the human NOD2 gene and an NF-κB–inducible secreted embryonic alkaline phosphatase reporter gene. An analogous assay with HEK-Blue NOD1 cells was used as the counter-screen, in terms of determination of the selectivity profile of these compounds by measuring their effects also on NOD1-dependent activation of NF-κB. Recognition of a NOD1/NOD2 agonist triggers a signaling pathway that leads to the activation of NF-κB and the production of secreted embryonic alkaline phosphatase. During these experiments, the cells were preincubated for 1 h with the synthesized compounds and also with the reference NOD2 antagonist **GSK669** (compound **13**) and NOD1 antagonist (**noditinib-1**), respectively, at 10 μM. Then, the cells were stimulated for 18 h with 2 μM MDP or 100 nM C12-iE-DAP, respectively, followed by spectrophotometric determination of the secreted embryonic alkaline phosphatase activity in the supernatant (Fig. 4). Compared to the untreated cells, the positive controls of the NOD1 agonist (C12-iE-DAP) and the NOD2 agonist (MDP) significantly increased their respective NF-κB transcriptional activities. These activities were suppressed by the NOD1 antagonist **noditinib-1** and the NOD2 antagonist **GSK669** (**13**), respectively.

For the derivatives **13**–**15**, which were characterized by spacers of different lengths between the benzimidazole and the benzoylamido moiety, and compound **19** as a retroamide analog of **13**, only **19** and compounds **13** and **15**, with spacers of two and three methylene units, respectively, diminished the NOD-agonist-induced increase in NF-κB transcriptional activity. Reduction of the length of the spacer to a single methylene unit (i.e., **14**) resulted in complete loss of this activity. Thus, spacers of at least two methylene units are required for the NOD-antagonist activity of this structural class of compounds.

The further analogs that incorporated distinct acyl/sulfonyl moieties as replacements for the phenyl ring were screened for these NOD1/2-antagonist activities to further explore the chemical space of **GSK669** (**13**). Compounds **27**, **28** and **29**, with the 4-pyridyl, 4-pyridylmethyl, and 3-pyridyl moieties, respectively, showed no NOD-antagonist activities through either of these receptors. However, introduction of the Boc-piperidine fragment in place of the phenyl group (i.e., **30**) yielded a dual NOD1/2 antagonist. The removal of Boc completely abolished this activity, as shown by compound **31**.

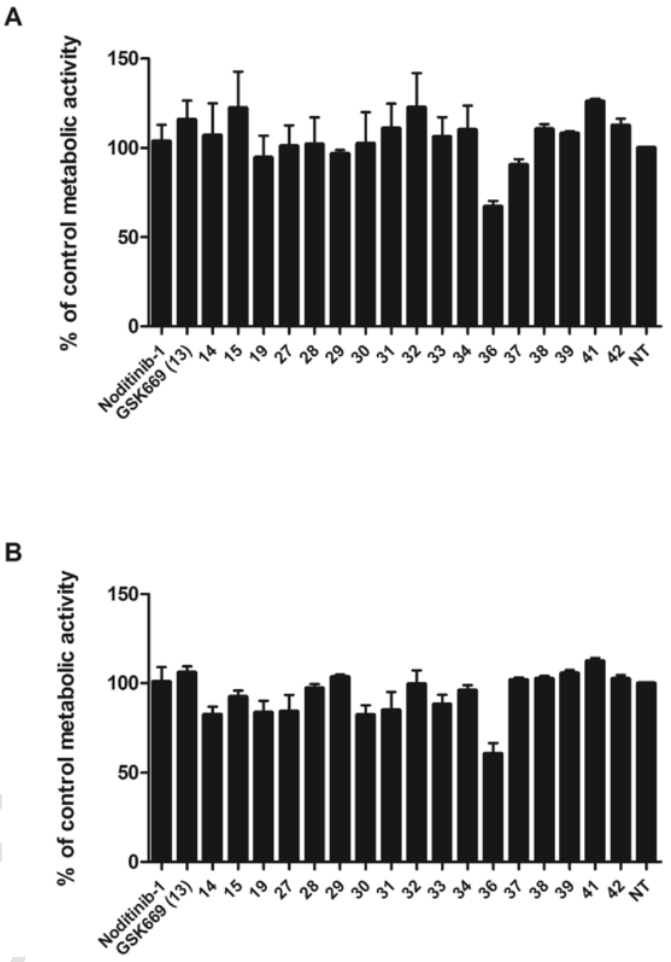

Fig. 3. MTS cell proliferation assay of synthesized compounds. Proliferation rates of HEK-Blue NOD2 **(A)** and HEK-Blue NOD1 **(B)** cells expressed as metabolic activities after 18 h treatment with the indicated synthesized compounds (20 μM). Data are means ± standard deviation of three independent experiments.

The replacement of the benzoyl moiety of **13** by arylsulfonyl structural features (for **32**–**34**) demonstrated promising NOD-antagonist activities, particularly for the phenylsulfonyl and naphthalenesulfonyl analogs **32** and **33**, respectively. Promising NOD-antagonist activities were also obtained by replacing the amide linkage of **13** with its methyleneamino isostere (i.e., **36**), while this was not the case for compound **37**.

To summarize, the data obtained in a single point assay indicate that most of the synthesized compounds disrupt both NOD1 and NOD2 signaling pathways.

2.3.3. NOD-antagonist IC_{50} values of the selected synthesized compounds

The compounds that showed significant NOD-antagonist activities in the preliminary screening were further investigated for their dose dependence and IC_{50} values (Table 1). The dose-dependence data supported the data for the single concentration of 10 μM. The NOD1-antagonist and NOD2-antagonist effects of all of the compounds tested here were dose dependent, and followed a non-linear semi-logarithmic model. Although unexpected, the NOD2 antagonist **GSK669** (**13**) that has been reported as NOD2 selective [20] showed relatively weak 4.5-fold selectivity (NOD1 vs. NOD2: IC_{50}, 27.6 vs. 6.2 μM). Con-

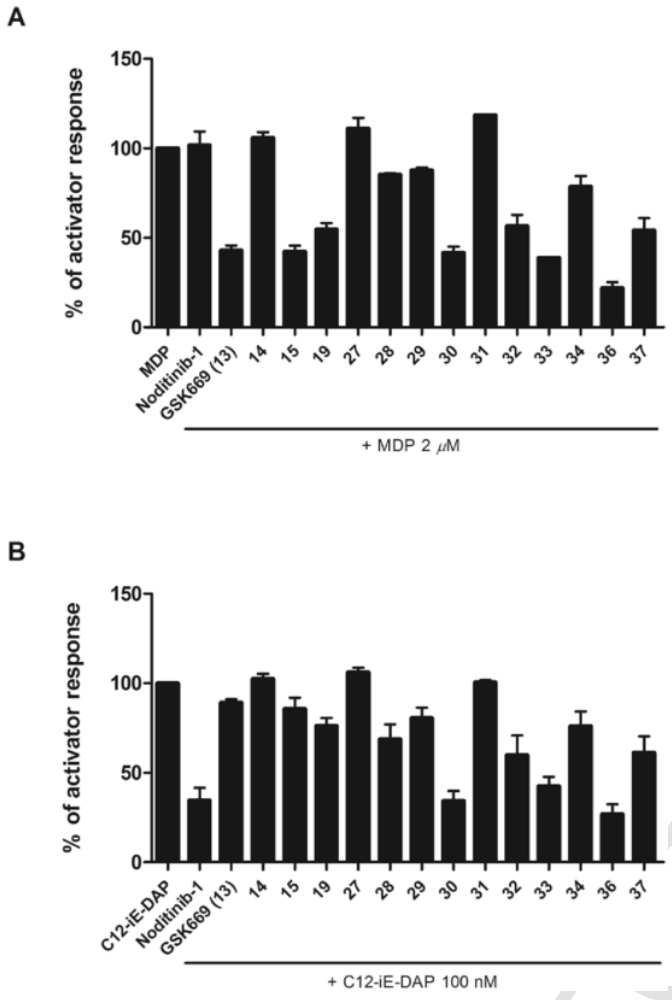

Fig. 4. The suppressive effect of synthesized NOD antagonists on NF-κB activation in HEK-Blue cells. NF-κB transcriptional activity of HEK-Blue NOD2 **(A)** and HEK-Blue NOD1 **(B)** cells expressed as secreted embryonic alkaline phosphatase activity after 1 h treatment with the indicated synthesized compounds (10 μM) before stimulation for 18 h with 2 μM MDP and 100 nM C12-iE-DAP, respectively. Data are means ± standard deviation of duplicates from three independent experiments.

versely, the NOD1 antagonist **noditinib-1** (**1**) showed submicromolar IC_{50} for NOD1 and was 71-fold less potent for NOD2 (IC_{50}, 0.771 vs. 54.9 μM, respectively), which is in agreement with its previously reported activities [15].

These synthesized compounds were designed based on the structure of **GSK669**. In contrast to the previous reports [20], these data revealed the relative nonselective nature of the benzimidazole scaffold in terms of NOD2 antagonism (i.e., vs. NOD1). Nevertheless, the data for these benzimidazole diamide analogs shed light on the SARs of this structural class of compounds. It appears that the replacements introduced generally interfered with both of the pathways in similar manners. Indeed, some compounds (i.e., **33**, **39**, **42**) showed even lower IC_{50} values for NOD1 antagonism *versus* NOD2 antagonism. This indicates that the initial NOD2 selectivity can be shifted toward NOD1 by replacing the amide linkage with its *N*-methylated counterpart (i.e., **39**, **42**) or by introducing the 5-(dimethylamino)naphthalenesulfonyl moiety in place of the phenyl ring (i.e., **33**).

Compound **33** emerged as one of the most potent and balanced dual antagonist of the series, with similar potencies in the low micromolar range toward NOD1 and NOD2 (IC_{50}, 2.68 vs. 6.20 μM, respectively). In terms of NOD2-antagonist activity, decreasing the length of the linker between the benzimidazole moiety and the benzoyl group of

Table 1
NOD1-antagonist and NOD2-antagonist activities of the selected compounds.

Compound	R	X	n	IC_{50} NOD1 [μM]	IC_{50} NOD2 [μM]
Noditinib-1	–	–		0.771	54.9
GSK669 (13)			1	27.6	6.2
14			0	n.d.	n.d.
15			2	17.7	5.7
19			1	12.4	8.8
27			1	n.d.	n.d.
28	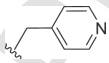		1	42.3	25.9
29			1	n.d.	n.a.
30	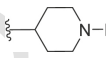		1	13.3	10.6
31			1	n.d.	n.d.
32			1	28.2	5.23
33	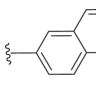		1	2.68	6.20
34			1	32.0	16.4
36			1	30.7	4.76
37			1	27.8	22.9
38			1	2.56	0.63
39	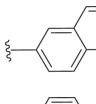		1	3.08	>20
41			2	9.25	5.12
42			2	1.66	5.08

n, number of methylene spacer units.

lead compound **GSK669** resulted in complete loss of activity, as shown by compound **14**. Conversely, lengthening the linker by one methylene unit (i.e., **15**) improved the antagonist activities a little for both the NOD1 and NOD2 targets (IC_{50}, 17.7 vs. 5.7 μM, respectively). Similarly to **14**, introduction of the pyridyl moiety (i.e., **27**, **29**) as a bioisosteric replacement of the phenyl ring resulted in analogs that were devoid of any activity. Moreover, the NOD2-antagonist activity was slightly reduced for **19** (IC_{50}, 12.4 vs. 8.8 μM, respectively), as a retro-amide analog of **GSK669**, and in the *N*-Boc-piperidine-incorporating analog, com-

pound **30** (IC_{50}, 13.3 vs. 10.6 μM, respectively). Removal of the Boc group from **30** (i.e., **31**) completely abolished the NOD2-antagonist properties. Conversely, replacement of the benzoyl moiety of the lead compound **GSK669** by the arylsulfonyl structural feature (i.e., **32**–**34**) resulted in a small increase in NOD2-antagonist activity compared to **GSK669**. In particular, promising NOD-antagonist activities were seen for the phenylsulfonyl derivative **32** (IC_{50}, 28.2 vs. 5.23 μM, respectively) and the naphthalenesulfonyl derivative **33** (IC_{50}, 2.68 vs. 6.20 μM, respectively). Promising data were also obtained by replacing the amide linkage of **GSK669** by its methyleneamino isostere, for compound **36** (IC_{50}, 30.7 vs. 4.76 μM, respectively). The nature of the linker type did not appear to be important for these antagonist activities. Similar NOD1-antagonist and NOD2-antagonist activities were seen for the analogs that incorporated the sulfonyl (**32**; IC_{50}, 28.2 vs. 5.23 μM, respectively), carbonyl (**13**; IC_{50}, 27.6 vs. 6.20 μM, respectively) and methylene (**36**; IC_{50}, 30.7 vs. 4.76 μM, respectively) moieties. Indeed, compound **36** was the most potent compound of the series in terms of NOD2 antagonism, with its activity surpassing that of the lead compound **GSK669** (IC_{50}, 4.76 vs. 6.2 μM, respectively). It should also be noted that this approach showed less encouraging results for compound **37**.

Finally, as methylation of the nitrogen adjacent to the phenyl moiety in **GSK669** resulted in increased activity [20], sulfonamides **32** and **33** were converted to their *N*-methylated counterparts **38** (NOD1 vs. NOD2: IC_{50}, 2.56 vs. 0.63 μM) and **39** (IC_{50}, 3.08 vs. >20 μM, respectively). Therefore, this *N*-methylation of **32** resulted in a nanomolar NOD2 antagonist, **38**, as the most potent of the series here, as expected. On the contrary, this conversion proved to be detrimental in terms of NOD2 antagonism for **39**, which was devoid of this activity, although its NOD1-antagonist activity was retained. Of note, examination of the SAR information obtained here for the first series of compounds (i.e., **15**, **32**) revealed that a spacer length of three methylene units plus replacement of the amide linkage by its *N*-methylated sulfonamide counterpart increased the selectivity of these compounds toward NOD2; therefore, compound **42** was prepared, whereby it combined these structural features. Of interest, **42** showed 17-fold improved activity *versus* NOD1, while its NOD2-antagonist activity was retained (IC_{50}, 1.66 vs. 5.08 μM, respectively).

Although compound **38** showed the lowest IC_{50} for NOD2, dose-dependence tests carried out from 0.25 μM to 20 μM produced ambiguous data at the highest concentration tested. Given that a 20 μM antagonist concentration was required for our functional characterization assays, **38** was excluded from further testing. Similar reasoning was used with **36**, which although it had potent NOD2-antagonist activity, it was cytotoxic at 20 μM, and hence it has not taken forward to the cell-based assays. Instead, **15** and **32** were chosen due to their micromolar IC_{50} values *versus* NOD2 and their moderate selectivity *versus* NOD1, while **33** was also selected based on its balanced activity for both of these targets.

2.3.4. Functional cell-based NOD-antagonist activities of the selected compounds

The primary screening in the HEK293 cells stably expressing exogenous NOD1 or NOD2 showed promising IC_{50} values for some of these selected compounds. Therefore, we next investigated whether their inhibition of NOD1 and NOD2 signaling was retained also in immortalized THP-1 cells and in primary cells (i.e., PBMCs) that express the endogenous functional NOD1 and NOD2 proteins.

Previous studies using different cell lines have demonstrated that stimulation of the NODs significantly increased IL-8 release [34–36]. The potential effects of chosen compounds were addresed in two experimental settings in THP-1 cells. Firstly, we investigated to what extent these NOD1 and NOD2 antagonists (**15**, **32**, **33**) blocked IL-8 release in THP-1 cells stimulated with MDP and C12-iE-DAP, respectively (Fig. 5A and B) [31]. Treatment of the THP-1 cells with these selected NOD antagonists at 20 μM alone did not result in substantial IL-8 release and saw only negligible TNF-α secretion (data not shown). Although the selected NOD antagonists are well-tolerated by HEK-Blue NOD1 and HEK-Blue NOD2 cells (Fig. 3), lactate dehydrogenase leakage was also assessed to evaluate their potential cytotoxicity for THP-1 cells (data not shown). Results confirmed that none of the compounds were cytotoxic at the maximum concentration tested (20 μM). Having established that these antagonists themselves are not cytotoxic and do not affect the cytokine secretion, their effects were investigated for NOD-agonist-induced IL-8 release. As expected, all of these compounds prevented MDP- and C12-iE-DAP -induced IL-8 release. Compounds **15**, **32**, and **33** showed similar inhibition of MDP-induced IL-8 secretion to that of the positive control **GSK669**. Similarly, they reduced IL-8 release from C12-iE-DAP-stimulated THP-1 cells, albeit to a smaller extent when compared to the positive control **noditinib-1**.

Moreover, NOD agonists are known to synergize with LPS, a Toll-like receptor 4 (TLR4) agonist, and with several other TLR agonists, in terms of enhanced production of pro-inflammatory cytokines [37–41]. Indeed, this double NOD/TLR stimulation reproduces the scenario of pathological conditions of infection/chronic inflammation. Therefore, we also asked whether they blocked the synergistic responses in THP-1 cells doubly stimulated with MDP or C12-iE-DAP and LPS (Fig. 5C and D), by measuring TNF-α release as described [31]. The decreased levels of TNF-α production induced by this combined stimulation of the THP-1 cells demonstrated suppression of NOD/TLR4 cross-talk by these selected compounds. These data are in agreement with a report by Uehara et al., who investigated NOD1/NOD2 suppression using RNA interference technology [34].

All of the tested compounds here also markedly suppressed TNF-α release from these doubly stimulated THP-1 cells for MDP plus LPS, to the levels induced by the TLR4 agonist alone (i.e., LPS), which was not seen for the combined stimulation with C12-iE-DAP plus LPS. While **noditinib-1** suppressed TNF-α release to the level induced by LPS alone, compound **32** only slightly decreased TNF-α release, and compounds **15** and **33** were only moderate inhibitors of TNF-α release. Importantly, these findings indicate that NOD/TLR4 crosstalk can be completely abolished by these NOD antagonists.

Compound **32** proved to be the most NOD2 selective of these NOD antagonists in the THP-1 cell assay, and therefore its actions were examined in primary cells that express the endogenous functional the NOD2 protein. Thus, immunosuppression by **32** was investigated for human PBMCs in the presence of MDP using cytometric bead array human cytokine kits (i.e., to measure IL-2, IL-4, IL-6, IL-10, TNF-α, IFN-γ levels) (Fig. 6). PBMCs are composed of 70–90% lymphocytes (T lymphocytes, B lymphocytes and natural killer cells), 10–20% monocytes and 1–2% dendritic cells [42]. As expected, stimulation with MDP did not affect the secretion of IL-2, IL-4, and IFN-γ from PBMCs; it should be noted that these cytokines are exclusively secreted by T lymphocytes [43]. On the other hand, the release of IL-6, IL-10, and TNF-α, primarily secreted by monocytes, were greatly increased by MDP; this indicates that MDP activated the monocyte fraction of PBMCs. These increases were diminished following pretreatment with compound **32**, which shows its potent inhibitory effects on IL-6, IL-10 and TNF-α release via its actions on NOD2. Compound **32** can thus also inhibit the NOD2 signaling pathway in primary cells, which provides further evidence of its functional activity and attests to its potential usefulness in further studies.

3. Conclusions

In conclusion, some substituted benzimidazoles have been identified as potent dual NOD1/NOD2 antagonists. The NOD2-antagonist activity of lead compound **GSK669** was improved by 10-fold by the moderately NOD2-selective compound **38**. On the other hand, compounds **33** and

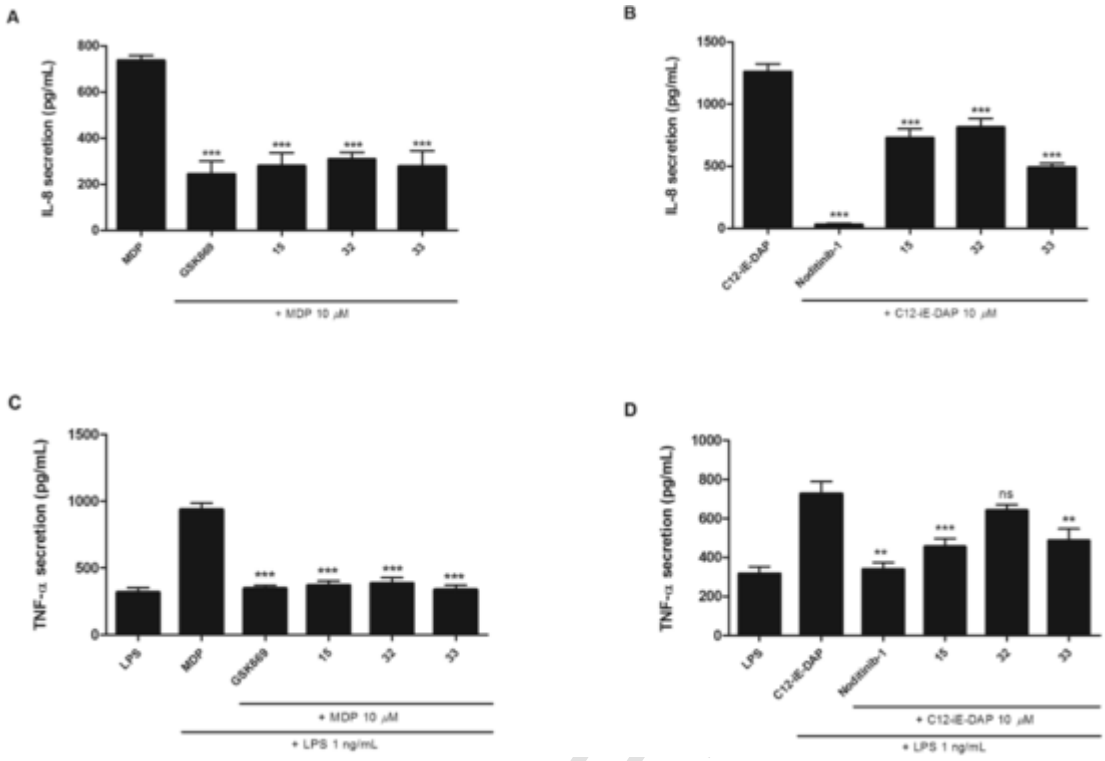

Fig. 5. (A, B) Suppression of NOD agonist-induced IL-8 secretion from THP-1 cells. Effects of the selected compounds on IL-8 secretion from MDP-stimulated **(A)** and C12-iE-DAP-stimulated **(B)** THP-1 cells following pre-treatment with the selected compounds (20 μM) for 1 h before addition of MDP or C12-iE-DAP (both at 10 μM) and an incubation for 20 h. Data are means ± standard deviation of duplicates from three independent experiments. *, $p < 0.05$; **, $p < 0.01$; ***, $p < 0.001$ *versus* MDP or C12-iE-DAP-treated cells. **(C, D)** NOD/TLR4 cross-talk modulation in THP-1 cells; effects of the selected compounds on NOD2/TLR4 **(C)** and NOD1/TLR4 **(D)** cross-talk. The THP-1 cells were preincubated for 1 h with selected compounds (20 μM) before stimulation with MDP or C12-iE-DAP (both at 10 μM) and 1 ng/mL LPS for 20 h, followed by determination of TNF-α release in the supernatant. Data are means ± standard deviation of duplicates from three independent experiments. ns, not significant ($p > 0.05$); **, $p < 0.01$; ***, $p < 0.001$ *versus* (MDP + LPS)- or (C12-iE-DAP + LPS)-treated cells.

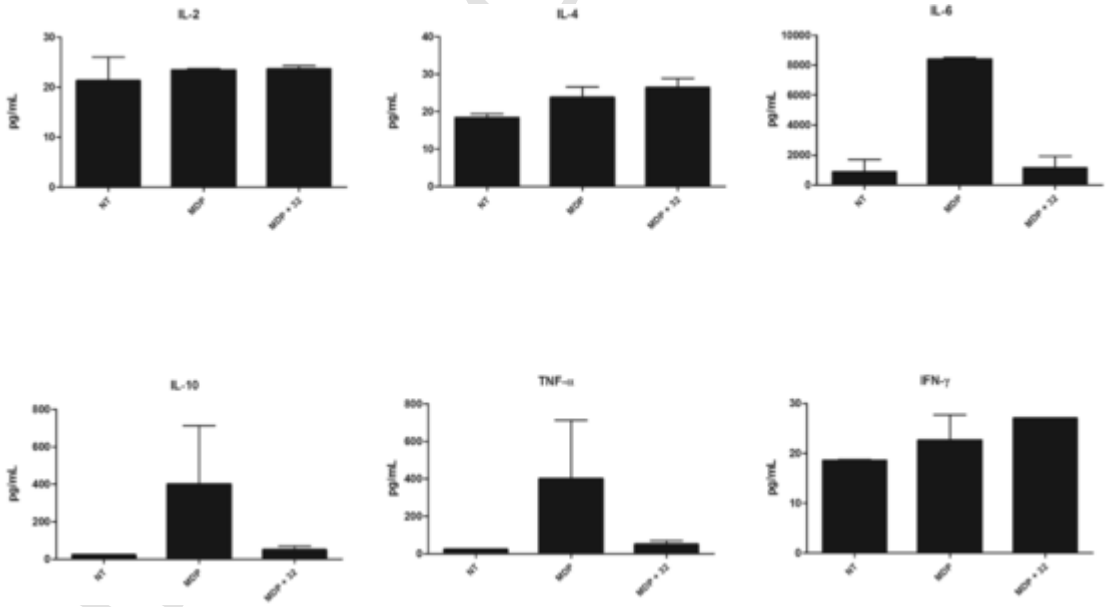

Fig. 6. Effects of compound **32** on cytokine release in MDP-stimulated PBMCs. PBMCs were pre-treated for 1 h with **32** (20 μM) and then MDP was added (2 μM). Control cells were treated with MDP (2 μM) alone. Cytokine release was determined after 18 h. Data are means ± standard deviation from two representative independent experiments.

42 show balanced dual NOD1/NOD2 activities for these targets. Compound **32** showed moderate NOD2 selectivity and retained its NOD-antagonist activity in functional assays. This ligand-based study has provided a deeper understanding of the SARs related to these NOD1-antagonist and NOD2-antagonist activities. A more thorough exploration of the chemical space will be needed to enhance the selectivity of these antagonists. The synthesized compounds described provide not only new chemical tools for further development of NOD antagonists, but also represent valuable research tools for further investigation of

the roles of these proteins in NOD-related diseases, as well as in normal host defense mechanisms.

4. Experimental section

4.1. General

Chemicals were obtained from Acros, Aldrich Chemical Co., Molekula and Fluka, and used without further purification. C12-iE-DAP (a synthetic NOD1 agonist) and MDP (NOD2 agonist) were obtained from InvivoGen, Inc., (San Diego, CA, USA); LPS (from *Escherichia coli* serotype 0127:B8) was from Sigma-Aldrich, Inc. (St. Louis, MO, USA). The NOD1 antagonist Noditinib-1 was synthesized as described [18]. The NOD2 antagonist GSK669 was synthesized as described [20]. Analytical TLC was performed on Merck 60 F254 silica gel plates (0.25 mm), using visualization with ultraviolet light and ninhydrin. Column chromatography was carried out on silica gel 60 (particle size 240–400 mesh). Melting points were determined on a Reichert hot stage microscope and are uncorrected. ^{1}H and ^{13}C NMR spectra were recorded at 400 MHz and 100 MHz, respectively, on a Bruker AVANCE III spectrometer in DMSO-d_6, $CDCl_3$, or MeOH-d_4 solution, with TMS as the internal standard. Spectra were assigned using gradient COSY and HSQC experiments. IR spectra were recorded on a PerkinElmer 1600 FT-IR spectrometer. Mass spectra were obtained using a VG-Analytical Autospec Q mass spectrometer. HPLC analyses were performed on an Agilent Technologies HP 1100 instrument with G1365B UV-VIS detector (210, 220 or 254 nm), using a Luna C18 column (4.6 × 150 mm) at a flow rate of 1 mL/min. The eluent was a mixture of 0.1% TFA in water (A) and acetonitrile (B), with a gradient of 30% B to 80% B from 0 to 30 min and 80% B to 90% B from 30 to 33 min. The purity of all pharmacologically investigated compounds was >95% as determined by RP-HPLC.

4.2. General procedures

4.2.1. Coupling

The corresponding Boc-protected amino acid (20.0 mmol), EDC × HCl (1.1 eq; 22.0 mmol), HOBt (1.1 eq; 22.0 mmol) and 1,2-diaminobenzene (1.1 eq; 22.0 mmol) were dissolved in THF (80 mL). Subsequently, triethylamine (1.5 eq; 30.0 mmol) was added dropwise and the reaction mixture was stirred overnight at room temperature. On completion of the reaction, the mixture was concentrated *in vacuo* and the residue dissolved in dichloromethane (200 mL). The organic phase was washed with water (2 × 70 mL) and brine (1 × 50 mL), then dried over anhydrous Na_2SO_4 and concentrated *in vacuo* to obtain sufficiently pure acylated *orto*-phenylenediamines.

4.2.2. Cyclization

The corresponding acylated *orto*-phenylenediamine (20.0 mmol) was dissolved in acetic acid (70 mL) and heated at 80 °C for 2 h. Upon completion of the reaction, which was monitored by TLC, the mixture was concentrated *in vacuo* and the residue dissolved in dichloromethane (200 mL). The organic phase was washed with saturated $NaHCO_3$ solution (3 × 50 mL), water (1 × 50 mL) and brine (1 × 50 mL), then dried over anhydrous Na_2SO_4 and concentrated *in vacuo* ot obtain sufficiently pure benzimidazoles.

4.2.3. N-alkylation of benzimidazole

Benzimidazole (5.0 mmol) was first dissolved in acetonitrile (40 mL); potassium carbonate (1.5 eq; 7.5 mmol) was then added and the mixture stirred for 15 min at room temperature. Subsequently, ethyl 2-bromoacetate (1.1 eq; 5.5 mmol) and a catalytical amount of TBAI (0.1 eq; 0.5 mmol) were added to the reaction mixture, which was heated overnight at reflux. Upon completion of the reaction, which was monitored by TLC, the mixture was concentrated *in vacuo* and the residue dissolved in dichloromethane (150 mL). The organic phase was washed with water (2 × 50 mL) and brine (1 × 50 mL), then dried over anhydrous Na_2SO_4 and concentrated *in vacuo*. The residue was purified by flash silica gel column chromatography (gradient elution; starting eluent: dichloromethane/methanol 30:1 *v/v*) to afford pure *N*-alkylated compounds.

4.2.4. Acidolytic cleavage of the Boc protecting group and subsequent acylation/sulfonylation

To an ice-chilled stirred mixture of *tert*-butyl carbamates (0.3 mmol) in AcOH (5 mL), 4M HCl/AcOH (3.4 eq; 1 mL) was added and the mixture allowed to warm to room temperature. After 3 h the reaction was complete and the solvent was evaporated *in vacuo*. Method A: the raw amine was dissolved in dry DMF (3 mL) and the corresponding carboxylic acid derivative (1.3 eq; 0.39 mmol), EDC (1.3 eq; 0.39 mmol), HOBt (1.3 eq; 0.39 mmol), a catalytic amount of DMAP and DIPEA (5 eq; 1.5 mmol) were added at 0 °C. The mixture was allowed to warm to room temperature and stirring was continued for 24 h. On completion, the reaction mixture was diluted with water (15 mL) and then washed with ethyl acetate (5 × 20 mL). The combined organic phases were washed with saturated $NaHCO_3$ solution (1 × 20 mL) and brine (1 × 20 mL), then dried over anhydrous Na_2SO_4 and the solvent was evaporated *in vacuo* to afford raw products, which were used in the next step without further purification; Method B: in case of compounds x-y, the raw amine was dissolved in THF (3 mL), then triethylamine (3.0 eq; 0.9 mmol) was added and the solution was cooled to 0 °C. Subsequently, the corresponding sulfonyl chloride (1.1 eq; 0.45 mmol) was added to the reaction mixture, which was stirred overnight at room temperature. On completion of the reaction, the mixture was concentrated *in vacuo* and the residue dissolved in dichloromethane (20 mL). The organic phase was washed with NaOH solution (pH~9; 1 × 10 mL) and brine (1 × 10 mL), then dried over anhydrous Na_2SO_4 and concentrated *in vacuo* to afford raw products, which were used in the next step without further purification.

4.2.5. Alkaline hydrolysis and subsequent coupling to 5-aminoindane

To a solution of ethyl ester (0.3 mmol) in THF (2 mL) was added 1M NaOH (5 eq; 1.5 mL) and the mixture stirred for 2 h at room temperature. Upon completion of the reaction which was monitored by TLC, the reaction mixture was acidified with 1M HCl to pH ~5 and then evaporated *in vacuo*. The raw acid was first dissolved in dry DMF (1 mL), then 5-aminoindane (1.5 eq; 0.45 mmol), EDC (1.5 eq; 0.45 mmol), HOBt (1.5 eq; 0.45 mmol), a catalytic amount of DMAP and DIPEA (3 eq; 0.9 mmol) were added at 0 °C. The mixture was allowed to warm to room temperature and stirring was continued for 24 h. On completion, the reaction mixture was poured into iced water (15 mL). The obtained precipitate was filtered off, washed with diethyl ether and dried at 60 °C overnight to afford pure compounds.

4.2.6. Reductive amination

To a solution of free amine (0.25 mmol) in 1,2-dichloroethane (5 mL) were added the corresponding aldehyde (1.0 eq; 1.0 mmol) and glacial acetic acid (1.0 eq; 1.0 mmol). The solution was bubbled with argon and stirred at room temperature for 2 h, then $NaBH(OAc)_3$ (1.6 eq; 0.4 mmol) was added and the mixture was stirred overnight. On completion of the reaction, the mixture was concentrated *in vacuo* and the residue dissolved in ethyl acetate (30 mL). The organic phase was washed with saturated $NaHCO_3$ solution (1 × 7 mL) and brine (1 × 10 mL), then dried over anhydrous Na_2SO_4 and concentrated *in vacuo*. The obtained residue was washed with diethyl ether and dried at 60 °C overnight to afford pure compounds.

4.2.7. N-methylation of sulfonamide NH

Sulfonamide (1.0 mmol) was first dissolved in DMF (2 mL); potassium carbonate (6 eq; 6.0 mmol) was then added and the mixture stirred for 15 min at room temperature. Subsequently, methyl iodide (3.0 eq; 3.0 mmol) was added to the reaction mixture, which was heated overnight at reflux. Upon completion of the reaction, which was monitored by TLC, the reaction mixture was poured into iced water (15 mL). The obtained precipitate was filtered off, washed with diethyl ether and dried at 60 °C overnight to afford pure *N*-methylated compounds.

4.3. Characterization of compounds

*4.3.1. Tert-butyl (3-((2-aminophenyl)amino)-3-oxopropyl)carbamate **(1)***

Orange amorphous solid, yield: 4.74 g (85%). ^{1}H NMR ($CDCl_3$, 400 MHz): δ = 1.43 (t, 3H, *J* = 7.2 Hz, -C<u>H</u>$_3$), 4.43 (q, 2H, *J* = 7.2 Hz, -C<u>H</u>$_2$CH$_3$), 7.15–7.20 (m, 3H, indole-<u>H</u> and Ar–<u>H</u>), 7.32–7.34 (m, 1H, indole-<u>H</u>), 7.45–7.47 (m, 1H, indole-<u>H</u>), 7.59–7.60 (m, 1H, Ar–<u>H</u>), 8.09–8.11 (m, 3H, Ar–<u>H</u>) ppm.

*4.3.2. Tert-butyl (2-((2-aminophenyl)amino)-2-oxoethyl)carbamate **(2)***

Brown amorphous solid, yield: 3.45 g (74%); m.p. 119–123 °C. ^{1}H NMR (DMSO-d_6, 400 MHz): δ = 1.39 (s, 9H, 3 × C<u>H</u>$_3$), 3.73 (d, 2H, *J* = 5.6 Hz, NHC<u>H</u>$_2$CO), 4.87 (s, 2H, N<u>H</u>$_2$), 6.50–6.55 (m, 1H, Ar–<u>H</u>), 6.69–6.71 (m, 1H, Ar–<u>H</u>), 6.89–6.92 (m, 1H, Ar–<u>H</u>), 7.04 (t, 1H, *J* = 6.0 Hz, N<u>H</u>CH$_2$), 9.08 (s, 1H, CON<u>H</u>) ppm. MS (ESI): *m/z* (%) = 266.2 (M + H)$^+$. HRMS Calcd for $C_{13}H_{20}N_3O_3$ *m/z*: 266.1505 (M + H)$^+$, found 266.1502.

*4.3.3. Tert-butyl (4-((2-aminophenyl)amino)-4-oxobutyl)carbamate **(3)***

Light brown amorphous solid, yield: 5.08 g (85%); m.p. 122–126 °C. ^{1}H NMR ($CDCl_3$, 400 MHz): δ = 1.44 (s, 9H, 3 × C<u>H</u>$_3$), 1.85–1.91 (m, 2H, CH$_2$C<u>H</u>$_2$CH$_2$), 2.04–2.44 (m, 2H, CH$_2$CH$_2$C<u>H</u>$_2$), 3.25–3.29 (m, 2H, C<u>H</u>$_2$CH$_2$CH$_2$), 4.05 (s, 2H, Ar-N<u>H</u>$_2$), 4.82 (s, 1H, N<u>H</u>Boc), 6.76–6.80 (m, 2H, Ar–<u>H</u>), 7.00–7.05 (m,1H, Ar–<u>H</u>), 7.35 (d, 1H, *J* = 7.6 Hz, Ar–<u>H</u>), 8.23 (s, 1H, ArN<u>H</u>CO) ppm. MS (ESI): *m/z* (%) = 294.2 (M + H)$^+$. HRMS Calcd for $C_{15}H_{24}N_3O_3$ *m/z*: 294.1818 (M + H)$^+$, found 294.1824.

*4.3.4. Tert-butyl (2-(1H-benzo[d]imidazole-2-yl)ethyl)carbamate **(4)***

Yellow amorphous solid, yield: 3.82 g (86%). ^{1}H NMR ($CDCl_3$, 400 MHz): δ = 1.41 (s, 9H, 3 × C<u>H</u>$_3$–C), 3.22 (t, 2H, *J* = 6.0 Hz, Ar-C<u>H</u>$_2$-CH$_2$), 3.67 (q, 2H, *J* = 6.0 Hz CH$_2$–C<u>H</u>$_2$–NH), 5.32 (s, 1H, CH$_2$-N<u>H</u>Boc), 7.24–7.29 (m, 2H, Ar–<u>H</u>), 7.55–7.76 (m, 2H, Ar–<u>H</u>), 8.84 (s, 1H, N<u>H</u>-benzimidazole) ppm.

*4.3.5. Tert-butyl ((1H-benz[d]imidazole-2-yl)methyl)carbamate **(5)***

Beige amorphous solid, yield: 4.16 g (100%); m.p. 184–186 °C. ^{1}H NMR (DMSO-d_6, 400 MHz): δ = 1.42 (s, 9H, 3 × C<u>H</u>$_3$), 4.36 (d, 2H, *J* = 5.6 Hz, NHC<u>H</u>$_2$), 7.14–7.16 (m, 2H, Ar–<u>H</u>), 7.44 (t, 1H, *J* = 5.2 Hz, N<u>H</u>), 7.49–7.51 (m, 2H, Ar–<u>H</u>), 12.23 (s, 1H, N<u>H</u>-Het) ppm. MS (ESI): *m/z* (%) = 248.1 (M + H)$^+$. HRMS Calcd for $C_{13}H_{18}N_3O_2$ *m/z*: 248.1399 (M + H)$^+$, found 248.1401.

*4.3.6. Tert-butyl (3-(1H-benz[d]imidazole-2-yl)propyl)carbamate **(6)***

Off-white amorphous solid, yield: 2.60 g (65%); m.p. 139–143 °C. ^{1}H NMR ($CDCl_3$, 400 MHz): δ = 1.47–1.52 (m, 9H, 3 × C<u>H</u>$_3$), 1.90–1.96 (m, 2H, CH$_2$CH$_2$C<u>H</u>$_2$), 2.96–2.99 (m, 2H, CH$_2$C<u>H</u>$_2$CH$_2$), 3.26–3.30 (m, 2H, -C<u>H</u>$_2$CH$_2$CH$_2$-), 4.89–4.92 (m, 1H, BocN<u>H</u>-), 7.22–7.26 (m, 2H, Ar–<u>H</u>), 7.61–7.62 (m, 2H, Ar–<u>H</u>), 11.20 (s, 1H, N<u>H</u>-Het) ppm. MS (ESI): *m/z* (%) = 276.2 (M + H)$^+$. HRMS Calcd for $C_{15}H_{22}N_3O_2$ *m/z*: 276.1712 (M + H)$^+$, found 276.1717.

*4.3.7. Ethyl 2-(2-(2-((tert-butoxycarbonyl)amino)ethyl)-1H-benzo[d]imidazole-1-yl)acetate **(7)***

Ochre amorphous solid, yield: 0.83 g (54%); m.p. 83–84 °C. ^{1}H NMR ($CDCl_3$, 400 MHz): δ = 1.26 (t, 3H, *J* = 7.2 Hz, CH$_2$C<u>H</u>$_3$), 1.42 (s, 9H, 3 × C<u>H</u>$_3$C), 3.01 (t, 2H, *J* = 6.0 Hz, ArC<u>H</u>$_2$CH$_2$), 3.72 (q, 2H, *J* = 6.0 Hz, CH$_2$C<u>H</u>$_2$NH), 4.23 (q, 2H, *J* = 7.2 Hz, C<u>H</u>$_2$CH$_3$), 4.83 (s, 1H, C<u>H</u>$_2$CO), 5.49 (s, 1H, CH$_2$N<u>H</u>Boc), 7.21–7.29 (m, 3H 3 × Ar–<u>H</u>), 7.72–7.74 (m, 1H, Ar–<u>H</u>) ppm. MS (ESI): *m/z* (%) = 348.2 (M + H)$^+$. HRMS Calcd for $C_{18}H_{26}N_3O_4$ *m/z*: 348.1923 (M + H)$^+$, found 348.1925.

*4.3.8. Ethyl 2-(2-(((tert-butoxycarbonyl)amino)methyl)-1H-benzo[d]imidazole-1-yl)acetate **(8)***

Yellow amorphous solid, yield: 204 mg (31%); m.p. 135–138 °C. ^{1}H NMR ($CDCl_3$, 400 MHz): δ = 1.27 (t, 3H, *J* = 7.2 Hz, C<u>H</u>$_3$CH$_2$), 1.45 (s, 9H, 3 × C<u>H</u>$_3$), 4.22 (q, 2H, *J* = 7.2 Hz, CH$_3$C<u>H</u>$_2$), 4.59 (d, 2H, *J* = 5.6 Hz, C<u>H</u>$_2$NH), 5.00 (s, 2H, C<u>H</u>$_2$N), 5.40 (s, 1H, N<u>H</u>Boc), 7.25–7.30 (m, 3H, Ar–<u>H</u>), 7.73–7.75 (m, 1H, Ar–<u>H</u>) ppm. MS (ESI): *m/z* (%) = 334.2 (M + H)$^+$. HRMS Calcd for $C_{17}H_{24}N_3O_4$ *m/z*: 334.1767 (M + H)$^+$, found 334.1760.

*4.3.9. Ethyl 2-(2-(3-((tert-butoxycarbonyl)amino)propyl)-1H-benzoimidazole-1-yl)acetate **(9)***

Brown amorphous solid, yield: 169 mg (23%); m.p. 118–120 °C. ^{1}H NMR ($CDCl_3$, 400 MHz): δ = 1.22 (t, 3H, *J* = 7.2 Hz, -CH$_2$C<u>H</u>$_3$), 1.38 (m, 9H, 3 × C<u>H</u>$_3$), 1.88 (qu, 2H, *J* = 7.2 Hz, CH$_2$C<u>H</u>$_2$CH$_2$), 2.75 (t, 2H, *J* = 7.6 Hz, CH$_2$CH$_2$C<u>H</u>$_2$), 3.02–3.06 (m, 2H, NHC<u>H</u>$_2$CH$_2$), 4.16 (q, 2H, *J* = 7.2 Hz, CH$_3$C<u>H</u>$_2$O-), 5.17 (s, 2H, NC<u>H</u>$_2$), 6.92 (t, 1H, *J* = 5.6 Hz, N<u>H</u>), 7.14–7.19 (m, 2H, Ar–<u>H</u>), 7.43–7.47 (m, 1H, Ar–<u>H</u>), 7.53–7.57 (m, 1H, Ar–<u>H</u>) ppm. MS (ESI): *m/z* (%) = 362.2 (M + H)$^+$. HRMS Calcd for $C_{19}H_{28}N_3O_4$ *m/z*: 362.2080 (M + H)$^+$, found 362.2075.

*4.3.10. Ethyl 2-(2-(benzamidoethyl)-1H-benzo[d]imidazole-1-yl)acetate **(10)***

Light brown amorphous solid, yield: 176 mg (41%); m.p. 84–85 °C. ^{1}H NMR ($CDCl_3$, 400 MHz): δ = 1.23 (t, 3H, *J* = 7.2 Hz, C<u>H</u>$_3$CH$_2$), 3.12 (t, 2H, *J* = 6.0 Hz, CH$_2$C<u>H</u>$_2$), 4.04 (q, 2H, *J* = 6.0 Hz, C<u>H</u>$_2$CH$_2$), 4.17 (q, 2H, *J* = 7.2 Hz, C<u>H</u>$_2$CH$_3$), 4.84 (s, 2H, NC<u>H</u>$_2$), 7.22–7.28 (m, 3H, Ar–<u>H</u>), 7.34–7.47 (m, 3H, Ar–<u>H</u>), 7.73–7.82 (m, 4H, 3 × Ar–<u>H</u> and N<u>H</u>CO) ppm. MS (ESI): *m/z* (%) = 352.2 (M + H)$^+$. HRMS Calcd for $C_{20}H_{22}N_3O_3$ *m/z*: 352.1661 (M + H)$^+$, found 352.1659.

*4.3.11. Ethyl 2-(2-(benzamidomethyl)-1H-benzo[d]imidazole-1-yl)acetate **(11)***

Off-white amorphous solid, yield: 142 mg (93%); m.p. 86–87 °C. ^{1}H NMR (DMSO-d_6, 400 MHz): δ = 1.08 (t, 3H, *J* = 7.2 Hz, CH$_3$), 3.96 (q, 2H, *J* = 7.2 Hz, C<u>H</u>$_2$CH$_3$), 4.75 (d, 2H, *J* = 6.0 Hz, C<u>H</u>$_2$NH), 5,28 (s, 2H, NC<u>H</u>$_2$), 7.18–7.24 (m, 2H, Ar–<u>H</u>), 7.45–7.64 (m, 3H, Ar–<u>H</u>), 7.88–7.96 (m, 4H, Ar–<u>H</u>), 9.17 (t, 1H, *J* = 5.6 Hz, N<u>H</u>) ppm. MS (ESI): *m/z* (%) = 338.1 (M + H)$^+$. HRMS Calcd for $C_{19}H_{20}N_3O_3$ *m/z*: 338.1505 (M-H)$^-$, found 338.1504.

*4.3.12. Ethyl 2-(2-(3-benzamidopropyl)-1H-benzo[d]imidazole-1-yl)acetate **(12)***

Light brown amorphous solid, yield: 81 mg (100%); m.p. 86–87 °C. ^{1}H NMR ($CDCl_3$, 400 MHz): δ = 1.18 (t, 3H, *J* = 7.2 Hz, C<u>H</u>$_3$CH$_2$-), 2.02–2.10 (m, 2H, C<u>H</u>$_2$), 2.85 (t, 2H, *J* = 7.6 Hz, C<u>H</u>$_2$), 3.38–3.43 (m, 2H, C<u>H</u>$_2$), 4.11–4.16 (m, 2H, C<u>H</u>$_2$CH$_3$), 5.19 (s, 2H, -NC<u>H</u>$_2$-), 7.15–7.20 (m, 2H, Ar–<u>H</u>), 7.43–7.64 (m, 3H, Ar–<u>H</u>), 7.85 (dd, 2H, *J* = 1.2 Hz, *J* = 8.8 Hz, Ar–<u>H</u>), 7.95 (dd, 2H, *J* = 1.2 Hz, *J* = 8.4 Hz, Ar–<u>H</u>), 8.62 (t, 1H, *J* = 5.2 Hz, N<u>H</u>) ppm. MS (ESI): *m/z* (%) = 364.2 (M-H)$^-$. HRMS Calcd for $C_{21}H_{22}N_3O_3$ *m/z*: 364.1661 (M-H)$^-$, found 364.1651.

4.3.13. N-(2-(1-(2-((2,3-dihydro-1H-indene-5-yl)amino)-2-oxoethyl)-1H-benzo[d]imidazole-2-yl)ethyl)benzamide ***(13)***

Off-white amorphous solid, yield: 49 mg (68%); m.p. 244–248 °C. ^{1}H NMR (DMSO-d_6, 400 MHz): δ = 1.94–2.02 (m, 2H, $CH_2C\underline{H}_2CH_2$), 2.77–2.82 (m, 4H, 2 × Ph-C$\underline{H}_2$), 3.14 (t, 2H, *J* = 7.2 Hz, C$\underline{H}_2CH_2$NH), 3.76–3.81 (m, 2H, $CH_2C\underline{H}_2$NH), 5.13 (s, 2H, NC$\underline{H}_2$CO), 7.13–7.20 (m, 3H, Ar–H), 7.29 (d, 1H, *J* = 7.6 Hz, Ar–H), 7.43–7.52 (m, 5H, Ar–H), 7.60–7.62 (m, 1H, Ar–H), 7.84 (d, 2H, *J* = 7.2 Hz, Ar–H), 8.70 (t, 1H, *J* = 5.6 Hz, CH_2NHCO), 10.43 (s, 1H, CONHAr) ppm. ^{13}C NMR (DMSO-d_6, 100 MHz): δ = 25.11, 26.75, 31.74, 32.43, 37.45, 46.07, 109.64, 115.47, 117.38, 118.46, 121.41, 121.79, 124.24, 127.08, 128.26, 131.16, 134.32, 135.57, 136.66, 138.91, 142.19, 144.25, 153.69, 165.15, 166.29 ppm. MS (ESI): *m/z* (%) = 437.2 (M-H)$^-$. HPLC (254 nm): 100%, t_R = 12.58 min. HRMS Calcd for $C_{27}H_{25}N_4O_2$ *m/z*: 437.1978 (M-H)$^-$, found 437.1969.

4.3.14. N-((1-(2-((1H-indene-5-yl)amino)-2-oxoethyl)-1H-benzo[d]imidazole-2-yl)methyl)benzamide ***(14)***

Light yellow amorphous solid, yield: 54 mg (44%); m.p. 278–280 °C. ^{1}H NMR (DMSO-d_6, 400 MHz): δ = 1.97–2.04 (m, 2H, $CH_2C\underline{H}_2CH_2$), 2.77–2.86 (m, 4H, 2 × C$\underline{H}_2$-Ar), 4.77 (d, 2H, *J* = 4.4 Hz, C$\underline{H}_2$NH-), 5.24 (s, 2H, C$\underline{H}_2$N), 7.11–7.24 (m, 3H, Ar–H), 7.40–7.62 (m, 7H, Ar–H), 7.87–7.95 (m, 2H, Ar–H), 9.16 (s, 1H, CH_2CONH), 10.36 (s, 1H, CONHAr) ppm. ^{13}C NMR (DMSO-d_6, 100 MHz): δ = 25.11, 31.73, 32.41, 36.20, 46.27, 109.90, 115.54, 117.42, 118.77, 121.77, 122.31, 124.16, 127.34, 127.53, 128.22, 128.35, 131.40, 133.63, 135.79, 136.55, 138.90, 141.80, 144.18, 152.50, 165.10, 166.36 ppm. MS (ESI): *m/z* (%) = 423.2 (M-H)$^-$. HPLC (254 nm): 100%, t_R = 11.63 min. HRMS Calcd for $C_{26}H_{23}N_4O_2$ *m/z*: 423.1821 (M-H)$^-$, found 423.1830.

4.3.15. N-(3-(1-(2-((2,3-dihydro-1H-indene-5-yl)amino)-2-oxoethyl)-1H-benzo[d]imidazole-2-yl)propyl)benzamide ***(15)***

Brown amorphous solid, yield: 10 mg (16%); m.p. 221–224 °C. ^{1}H NMR (DMSO-d_6, 400 MHz): δ = 1.95–2.07 (m, 2H, C$\underline{H}_2$-Ar), 2.15 (s, 2H, $CH_2C\underline{H}_2CH_2$), 2.80 (t, 4H, *J* = 7.2 Hz, 2 × C$\underline{H}_2$-Ar), 2.92 (t, 2H, *J* = 7.2 Hz, C$\underline{H}_2CH_2CH_2$), 3.41–3.46 (m, 2H, $CH_2CH_2C\underline{H}_2$), 5.09 (s, 2H, COC$\underline{H}_2$N), 7.14–7.21 (m, 3H, Ar–H), 7.28 (d, 1H, *J* = 8.0 Hz, Ar–H), 7.40–7.60 (m, 6H, Ar–H), 7.82 (d, 2H, *J* = 8.8 Hz, Ar–H), 8.64 (t, 1H, *J* = 5.6 Hz, NHCOCH$_2$), 10.40 (s, 1H, CONHAr) ppm. ^{13}C NMR (DMSO-d_6, 100 MHz): δ = 24.16, 25.12, 26.39, 31.75, 32.42, 109.58, 115.49, 117.40, 118.28, 121.31, 121.62, 124.24, 127.09, 128.17, 130.96, 134.61, 136.65, 138.90, 142.09, 142.15, 144.24, 155.49, 165.17, 166.25, 170.24 ppm. MS (ESI): *m/z* (%) = 451.2 (M-H)$^-$. HPLC (254 nm): 100%, t_R = 12.63 min. HRMS Calcd for $C_{28}H_{27}N_4O_2$ *m/z*: 451.2134 (M-H)$^-$, found 451.2144.

4.3.16. N^1-(2-aminophenyl)-N^4-phenylsuccinamide ***(16)***

Off-white amorphous solid, yield: 2.15 g (73%); m.p. 195–199 °C. ^{1}H NMR (DMSO-d_6, 400 MHz): δ = 2.64–2.65 (m, 4H, 2 × C$\underline{H}_2$), 4.88 (s, 2H, NH_2), 6.49–6.53 (m, 1H, Ar–H), 6.68–6.70 (m, 1H, Ar–H), 6.86–6.91 (m, 1H, Ar–H), 7.00 (s, 1H, Ar–H), 7.11–7.13 (m, 1H, Ar–H), 7.29 (t, 2H, *J* = 8.0 Hz, Ar–H) 7.59 (d, 2H, *J* = 7.8 Hz, Ar–H), 9.19 (s, 1H, CONH), 10.00 (s, 1H, PhNHCO) ppm. MS (ESI): *m/z* (%) = 282.1 (M-H)$^-$. HRMS Calcd for $C_{16}H_{16}N_3O_2$ *m/z*: 282.1243 (M + H)$^+$, found 282.1246.

4.3.17. 3-(1H-benzo[d]imidazole-2-yl)-N-phenylpropanamide ***(17)***

White amorphous solid, yield: 574 mg (100%); m.p. 232–235 °C. ^{1}H NMR (DMSO-d_6, 400 MHz): δ = 2.91 (t, 2H, *J* = 7.2 Hz, C$\underline{H}_2CH_2$), 3.13 (t, 2H, *J* = 7.2 Hz, $CH_2C\underline{H}_2$), 7.00 (t, 1H, *J* = 7.2 Hz, Ar–H), 7.07–7.11 (m, 2H, Ar–H), 7.25–7.29 (m, 2H, Ar–H), 7.44–7.46 (m, 2H, Ar–H), 7.60 (d, 2H, *J* = 7.6 Hz, Ar–H), 10.34 (s, 1H, CONH), 12.66 (s, 1H, NH-Het) ppm. MS (ESI): *m/z* (%) = 264.1 (M-H)$^-$. HRMS Calcd for $C_{16}H_{14}N_3O$ *m/z*: 264.1137 (M-H)$^-$, found 264.1142.

4.3.18. Ethyl 2-(2-(3-oxo-3-(phenylamino)propyl)-1H-benzo[d]imidazole-1-yl)acetate ***(18)***

Brown amorphous solid, yield: 153 mg (69%); m.p. 93–96 °C. ^{1}H NMR ($CDCl_3$, 400 MHz): δ = 1.23 (t, 3H, *J* = 7.2 Hz, C$\underline{H}_3CH_2$), 2.94 (t, 2H, *J* = 7.2 Hz, C$\underline{H}_2CH_2$), 3.08 (t, 2H, *J* = 7.2 Hz, $CH_2C\underline{H}_2$), 4.18 (q, 2H, *J* = 7.2 Hz, C$\underline{H}_2CH_3$), 5.25 (s, 2H, NC$\underline{H}_2$), 7.02 (t, 1H, *J* = 7.2 Hz, Ar–H),7.14–7.20 (m, 2H, Ar–H), 7.48 (d, 1H, *J* = 6.8 Hz, Ar–H), 7.26–7.30 (m, 2H, Ar–H), 7.54–7.61 (m, 3H, Ar–H), 10.09 (s, 1H, CONH) ppm. MS (ESI): *m/z* (%) = 250.2 (M-H)$^-$. HRMS Calcd for $C_{20}H_{20}N_3O_3$ *m/z*: 350.1505 (M-H)$^-$, found 350.1513.

4.3.19. 3-(1-(2-((2,3-dihydro-1H-indene-5-yl)amino)-2-oxoethyl)-1H-benzo[d]imidazole-2-yl)-N-phenylpropanamide ***(19)***

Off-white amorphous solid, yield: 140 mg (36%); m.p. 239–241 °C. ^{1}H NMR (DMSO-d_6, 400 MHz): δ = 1.95–2.02 (m, 2H, $CH_2C\underline{H}_2CH_2$), 2.77–2.82 (m, 4H, 2 × PhC$\underline{H}_2$), 2.98 (t, 2H, *J* = 7.2 Hz, $CH_2C\underline{H}_2$CO), 3.14 (t, 2H, *J* = 7.2 Hz, C$\underline{H}_2CH_2$CO), 5.15 (s, 2H, NCH_2), 7.01 (t, 1H, *J* = 7.6 Hz, Ar–H), 7.14–7.20 (m, 3H, Ar–H), 7.25–7.31 (m, 3H, Ar–H), 7.47–7.60 (m, 5H, Ar–H), 10.12 (s, 1H, NH), 10.44 (s, 1H, NH) ppm. ^{13}C NMR (DMSO-d_6, 100 MHz): δ = 21.98, 25.11, 31.74, 32.43, 33.24, 109.64, 115.46, 117.37, 118.29, 118.92, 121.32, 121.69, 122.95, 124.24, 128.65, 135.76, 136.69, 138.89, 139.23, 142.00, 144.25, 155.09, 165.20, 170.20, 177.22 ppm. MS (ESI): *m/z* (%) = 437.2 (M-H)$^-$. HPLC (254 nm): 100%, t_R = 13.87 min. HRMS Calcd for $C_{27}H_{25}N_4O_2$ *m/z*: 437.1978 (M + H)$^+$, found 437.1972.

4.3.20. N-(2-(1-(2-((2,3-dihydro-lH-indene-5-yl)amino)-2-oxoethyl)-1H-benzo[d]imidazol-2-yl)ethyl)isonicotinamide ***(27)***

Brown amorphous solid, yield: 86 mg (82%); m.p. 150–154 °C. ^{1}H NMR ($CDCl_3$, 400 MHz): δ = 1.90–2.02 (m, 2H, $CH_2C\underline{H}_2CH_2$), 2.73–2.77 (m, 4H 2 × Ph-C$\underline{H}_2CH_2$), 3.04 (t, 2H, *J* = 6.8 Hz, Ar-C$\underline{H}_2$-CH_2), 3.58 (t, 2H, *J* = 6.8 Hz, CH_2–C$\underline{H}_2$–NH), 5.03 (s, 1H, N–C$\underline{H}_2$–CO), 7.03–7.05 (m, 2H, Ar–H), 7.14–7.19 (m, 4H, 4 × Ar–H), 7.32–7.36 (m, 3H, 2 × Ar–H in CH_2–NH–CO), 7.53–7.55 (m, 1H, NH), 7.61–7.63 (m, 1H, Ar–H), 8.50–8.51 (m, 1H, Ar–H) ppm. ^{13}C NMR (DMSO-d_6, 100 MHz): δ = 22.60, 26.68, 28.09, 33.26, 33.90, 38.82, 47.38, 110.80, 117.61, 119.31, 119.56, 123.65, 124.03, 125.41, 136.69, 137.33, 141.73, 142.96, 146.10, 155.07, 167.08, 173.63 ppm. MS (ESI): *m/z* (%) = 440.2 (M + H)$^+$. HPLC (254 nm): 94.4%, t_R = 6.53 min. HRMS Calcd for $C_{26}H_{26}N_5O_2$ *m/z*: 440.1999 (M + H)$^+$, found 440.2005.

4.3.21. N-(2,3-dyhidro-1H-indene-5-yl)-2-(2-(2-(2-(pyridine-4-yl)acetamido)ethyl)-1H-benzo[d]imidazole-1-yl)acetamide ***(28)***

Orange-brown amorphous solid, yield: 27 mg (39%); m.p. 87–90 °C. ^{1}H NMR (MeOD, 400 MHz): δ = 1.93–2.00 (m, 2H, $CH_2C\underline{H}_2CH_2$), 2.74–2.79 (m, 4H, 2 × Ph-C$\underline{H}_2CH_2$), 3.05 (t, 2H, *J* = 7.2 Hz, Ar-C$\underline{H}_2$-CH_2), 3.57–3.65 (m, 2H, CH_2–C$\underline{H}_2$–NH), 5.01 (s, 1H, N–C$\underline{H}_2$–CO), 5.05 (s, 1H, Py-C$\underline{H}_2$-CO), 7.04–7.06 (m, 2H, 2 × Ar–H), 7.12–7.20 (m, 4H, 4 × Ar–H), 7.33–7.37 (m, 2H, 2 × Ar–H), 7.54–7.56 (m, 2H, 2 × Ar–H), 8.20–8.21 (m, 1H, Ar–H) ppm. ^{13}C NMR (DMSO-d_6, 100 MHz): δ = 22.61, 26.68, 27.87, 28.08, 33.26, 33.90, 38.82, 47.39, 110.82, 110.85, 117.61, 119.31, 119.35, 119.57, 123.65, 123.70, 124.04, 124.08, 125.41, 126.17, 136.69, 137.35, 141.72, 142.96, 146.09, 149.89, 155.08, 167.09, 173.62 ppm. MS (ESI): *m/z* (%) = 452.2 (M-H)$^-$. HPLC (254 nm): 87.1%, t_R = 6.50 min. HRMS Calcd for $C_{27}H_{26}N_5O_2$ *m/z*: 452.2087 (M-H)$^-$, found 452.2077.

*4.3.22. Tert-butyl 4-((2-(1-(2-((2,3-dihydro-1H-indene-5-yl)amino)-2-oxoethyl)-1H-benzo[d]imidazole-2-yl)ethyl)carbamoyl)piperidine-1-carboxylate **(29)***

Brown amorphous solid, yield: 13 mg (28%); m.p. >300 °C. ^{1}H NMR ($CDCl_3$, 400 MHz): δ = 1.96–2.04 (m, 2H, $CH_2C\underline{H}_2CH_2$), 2.77–2.81 (m, 4H, 2 × Ph-C$\underline{H}_2CH_2$), 3.86 (t, 2H, *J* = 6.8 Hz CH_2–C$\underline{H}_2$–NH), 5.14 (s, 1H, N–C$\underline{H}_2$–CO), 7.05–7.07 (m, 1H, Ar–$\underline{H}$), 7.17–7.24 (m, 3H, 3 × Ar–$\underline{H}$), 7.36–7.43 (m, 2H, 3 × Ar–$\underline{H}$), 7.56–7.58 (m, 1H, Ar–$\underline{H}$), 8.13 (d, 1H, *J* = 8.0 Hz, Ar–$\underline{H}$), 8.57–8.58 (m, 1H, Ar–$\underline{H}$), 8.87 (d, 1H, *J* = 1.6 Hz, Ar–$\underline{H}$) ppm. ^{13}C NMR (DMSO-d_6, 100 MHz): δ = 26.96, 27.90, 33.25, 33.91, 39.51, 47.45, 110.86, 117.50, 119.30, 119.46, 123.70, 124.08, 125.08, 125.36, 137.04, 137.34, 141.66, 143.00, 146.04, 149.22, 152.57, 155.09, 167.06, 168.01 ppm. MS (ESI): *m/z* (%) = 438.2 (M-H)$^-$. HPLC (254 nm): 100%, t_R = 4.56 min. HRMS Calcd for $C_{26}H_{24}N_5O_2$ *m/z*: 438.1930 (M-H)$^-$, found 438.1919.

*4.3.23. Tert-butyl 4-((2-(1-(2-((2,3-dihydro-1H-indene-5-yl)amino)-2-oxoethyl)-1H-benzo[d]imidazole-2-yl)ethyl)carbamoyl)piperidine-1-carboxylate **(30)***

Orange-brown amorphous solid, yield: 87 mg (42%); m.p. 90–93 °C. ^{1}H NMR (MeOD, 400 MHz): δ = 1.40 (s, 9H, 3 × C$\underline{H}_3$–C), 1.59–1.62 (m, 2H, CH_2–C$\underline{H}_2$–CH_2), 1.96–2.05 (m, 2H, CH_2–C$\underline{H}_2$–CH_2), 2.55–2.83 (m, 8H, 2 × CH_2–C$\underline{H}_2$–N in 2 × C$\underline{H}_2$), 3.09 (t, 2H, *J* = 6.8 Hz, Ar-C$\underline{H}_2$-CH_2), 3.59.-3.64 (m, 2H, CH_2–C$\underline{H}_2$–NH), 5.10 (s, 1H, N–C$\underline{H}_2$–CO), 7.09 (d, 1H, *J* = 8.0 Hz, Ar–$\underline{H}$) 7.19–7.25 (m, 3H, 3 × Ar–$\underline{H}$), 7.37–7.41 (m, 2H, 2 × Ar–$\underline{H}$), 7.56–7.58 (m, 1H, Ar–$\underline{H}$) ppm. ^{13}C NMR (DMSO-d_6, 100 MHz): δ = 26.71, 28.08, 28.67, 29.57, 33.26, 33.94, 38.67, 38.82, 43.87, 47.47, 81.08, 110.83, 117.58, 119.28, 119.53, 123.67, 123.71, 124.07, 125.41, 136.69, 137.39, 141.73, 142.91, 146.09, 155.10, 156.38, 167.13, 177.71 ppm. MS (ESI): *m/z* (%) = 544.3 (M-H)$^-$. HPLC (254 nm): 96.7%, t_R = 13.36 min. HRMS Calcd for $C_{31}H_{38}N_5O_4$ *m/z*: 544.2924 (M-H)$^-$, found 544.2929.

*4.3.24. 4-(2-(1-(2-((2,3-Dihydro-1H-indene-5-yl)amino)-2-oxoethyl)-1-H-benzo[d]imidazole-2-yl)ethyl)carbamoylpiperidine-1-yl chloride **(31)***

Brown oil, yield: 40 mg (75%). ^{1}H NMR (MeOD, 400 MHz): δ = 1.58–1.68 (m, 2H, C$\underline{H}_2$), 1.79–1.98 (m,6H, 3 × CH_2), 2.70–2.72 (m, 4H, 2 × CH_2), 2.78–2.84 (m, 2H, CH_2–C$\underline{H}_2$–N, 3.32–3.38 (m, 2H, Ar-C$\underline{H}_2$-CH_2), 3.58–3.64 (m, 2H, CH_2–C$\underline{H}_2$–NH), 5.40 (s, 1H, N–C$\underline{H}_2$–CO), 7.00–7.02 (m, 1H, Ar–$\underline{H}$), 7.21 (d, 1H, *J* = 8.0 Hz, Ar–$\underline{H}$), 7.36 (s, 1H, Ar–$\underline{H}$), 7.46 (d, 2H, *J* = 7.6 Hz, 2 × Ar–$\underline{H}$), 7.67–7.72 (m, 2H, 2 × Ar–$\underline{H}$) ppm. ^{13}C NMR (DMSO-d_6, 100 MHz): δ = 22.71, 26.49, 26.70, 27.46, 33.29, 33.94, 38.03, 40.73, 44.34, 113.55, 115.56, 117.48, 117.52, 119.45, 119.50, 125.49, 127.45, 127.49, 127.72, 137.25, 141.94, 146.17, 164.83, 176.47 ppm. MS (ESI): *m/z* (%) = 444.2 (M-H)$^-$. HPLC (254 nm): 88.8%, t_R = 3.72 min. HRMS Calcd for $C_{26}H_{30}N_5O_2$ *m/z*: 444.2400 (M-H)$^-$, found 444.2394.

*4.3.25. N-(2,3-dihydro-1H-indene-5-yl)-2-(2-(2-(phenylsulfonamido)ethyl)-1H-benzo [d]imidazole-l-yl)acetamide **(32)***

Yellow-brown amorphous solid, yield: 24 mg (56%); m.p. 106–110 °C. ^{1}H NMR ($CDCl_3$, 400 MHz): δ = 1.99 (t, 2H, *J* = 6.8 Hz, $CH_2C\underline{H}_2CH_2$), 2.80–2.82 (m, 4H, 2 × Ph-C$\underline{H}_2CH_2$), 2.98–3.01 (m, 2H, Ar-C$\underline{H}_2$-CH_2), 3.25–3.27 (m, 2H, CH_2–C$\underline{H}_2$–NH), 5.05 (s, 1H, N–C$\underline{H}_2$–CO), 7.17–7.29 (m, 4H, 4 × Ar–H), 7.45–7.63 (m, 6H, 5 × Ar–H in CH_2–N$\underline{H}$–SO_2), 7.76–7.92 (m, 3H, 3 × Ar–H), 10.39 (s, 1H, CO–N$\underline{H}$-Ar) ppm. ^{13}C NMR (DMSO-d_6, 100 MHz): δ = 25.12, 27.27, 31.75, 32.44, 40.52, 45.96, 109.65, 115.48, 117.39, 118.42, 121.43, 121.84, 124.25, 126.47, 129.23, 132.45, 135.48, 136.65, 138.93, 140.10, 141.99, 144.26, 152.98, 165.02 ppm. MS (ESI): *m/z* (%) = 473.2 (M-H)$^-$. HPLC (254 nm): 100%, t_R = 11.60 min. HRMS Calcd for $C_{26}H_{25}N_4O_3S$ *m/z*: 473.1647 (M-H)$^-$, found 473.1656.

*4.3.26. N-(2,3-dihydro-1H-indene-5-yl)-2-(2-(2-((5-(dimethylamino)naphthalene)-1-sulfonamido)ethyl)-1H-benzo[d]imidazole-1-yl)acetamide **(33)***

Brown amorphous solid, yield: 55 mg (81%); m.p. 105–110 °C. ^{1}H NMR ($CDCl_3$, 400 MHz): δ = 1.97–2.03 (m, 2H, $CH_2C\underline{H}_2CH_2$), 2.73–2.88 (m, 10H, 2 × Ph-C$\underline{H}_2CH_2$ in 2 × CH_3–N), 2.99–3.01 (m, 2H, *J* = 6.0 Hz, Ar-C$\underline{H}_2$-CH_2), 3.27–3.32 (m, 2H, CH_2–C$\underline{H}_2$–NH), 5.02 (s, 1H, N–C$\underline{H}_2$–CO), 7.15–7.29 (m, 5H, 4 × Ar–$\underline{H}$ in CH_2–N$\underline{H}$–SO_2), 7.43–7.60 (m, 5H, 5 × Ar–$\underline{H}$), 8.13–8.15 (m, 2H, 2 × Ar–$\underline{H}$), 8.27 (d, 1H, *J* = 8.4 Hz, 1 × Ar–$\underline{H}$), 8.44 (d, 1H, *J* = 8.0 Hz, 1 × Ar–$\underline{H}$), 10.38 (s, 1H, CO–N$\underline{H}$-Ar) ppm. ^{13}C NMR (DMSO-d_6, 100 MHz): δ = 25.12, 27.37, 31.75, 32.44, 40.50, 45.02, 45.94, 109.60, 115.11, 115.50, 117.41, 118.38, 118.89, 121.45, 121.85, 123.53, 124.25, 127.88, 128.39, 128.94, 129.02, 129.50, 135.37, 135.46, 136.60, 138.96, 141.89, 144.26, 151.33, 152.99, 164.99 ppm. MS (ESI): *m/z* (%) = 566.2 (M-H)$^-$. HPLC (254 nm): 95.4%, t_R = 11.55 min. HRMS Calcd for $C_{32}H_{32}N_5O_3S$ *m/z*: 566.2226 (M-H)$^-$, found 566.2229.

*4.3.27. N-(2,3-dihydro-1H-indene-5-yl)-2-(2-(2-(pyridine-3-sulfonamido)ethyl)-1H-benzo[d]imidazole-l-yl)acetamide **(34)***

Brown amorphous solid, yield: 41 mg (46%); m.p. 142–144 °C. ^{1}H NMR ($CDCl_3$, 400 MHz): δ = 1.99 (t, 2H, *J* = 7.2 Hz, $CH_2C\underline{H}_2CH_2$), 2.78–2.82 (m, 4H, 2 × Ph-C$\underline{H}_2CH_2$), 3.00–3.04 (t, 2H, *J* = 7.2 Hz, Ar-C$\underline{H}_2$-CH_2), 3.35 (s, 2H, CH_2–C$\underline{H}_2$–NH), 5.06 (s, 1H, N–C$\underline{H}_2$–CO), 7.15–7.19 (m, 3H, 2 × Ar–$\underline{H}$ in CH_2–N$\underline{H}$–SO_2), 7.27–7.29 (m, 1H, 1 × Ar–$\underline{H}$), 7.45–7.49 (m, 2H, 2 × Ar–$\underline{H}$), 7.54–7.60 (m, 2H, 2 × Ar–$\underline{H}$), 8.13–8.19 (m, 2H, 2 × Ar–$\underline{H}$), 8.79 (d, 1H, *J* = 4.0 Hz, 1 × Ar–$\underline{H}$), 8.97 (d, 1H, *J* = 0.8 Hz, 1 × Ar–$\underline{H}$), 10.40 (s, 1H, CO–N$\underline{H}$-Ar) ppm. ^{13}C NMR (DMSO-d_6, 100 MHz): δ = 22.58, 25.12, 27.28, 31.75, 32.43, 40.43, 45.98, 109.65, 115.49, 117.40, 118.44, 121.44, 121.86, 124.25, 134.51, 135.49, 136.55, 136.62, 138.95, 141.98, 144.27, 147.03, 153.03, 165.04, 169.36 ppm. MS (ESI): *m/z* (%) = 474.2 (M-H)$^-$. HPLC (254 nm): 93.0%, t_R = 8.38 min. HRMS Calcd for $C_{25}H_{24}N_5O_3S$ *m/z*: 474.1600 (M-H)$^-$, found 474.1605.

*4.3.28. Tert-butyl (2-(1-(2-((2,3-dihydro-1H-indene-5-yl)amino)-2-oxoethyl)-1H-benzo[d]imidazole-2-yl)ethyl)carbamate **(35)***

Brown amorphous solid, yield: 193 mg (42%); m.p. 111–115 °C. ^{1}H NMR ($CDCl_3$, 400 MHz): δ = 1.26 (s, 9H, 3 × C$\underline{H}_3$–C), 2.01–2.08 (m, 2H, $CH_2C\underline{H}_2CH_2$), 2.80–2.86 (m, 4H, 2 × Ph-C$\underline{H}_2CH_2$), 3.11 (t, 2H, *J* = 6.0 Hz, Ar-C$\underline{H}_2$-CH_2), 3.57 (k, 2H, *J* = 6.4 Hz, CH_2–C$\underline{H}_2$–NH), 4.94 (s, 1H, N–C$\underline{H}_2$–CO), 5.21 (t, 1H, *J* = 6.4 Hz, CH_2-N$\underline{H}$Boc), 7.11 (d, 1H, *J* = 8.0 Hz, Ar–$\underline{H}$), 7.24–7.31 (m, 1H, Ar–$\underline{H}$), 7.38–7.40 (m, 1H, Ar–$\underline{H}$), 7.45 (s, 1H, Ar–$\underline{H}$), 7.70–7.71 (m, 1H, Ar–$\underline{H}$), 9.05 (s, 1H, CO–N$\underline{H}$-Ar) ppm. ^{13}C NMR ($CDCl_3$, 100 MHz): δ = 25.59, 28.19, 28.22, 32.35, 32.89, 38.59, 80.07, 109.66, 117.03, 118.71, 119.54, 122.64, 123.26, 124.25, 135.46, 135.51, 140.76, 142.59, 144.89, 156.43, 156.47 ppm. MS (ESI): *m/z* (%) = 433.2 (M-H)$^-$. HRMS Calcd for $C_{25}H_{29}N_4O_3$ *m/z*: 433.2240 (M-H)$^-$, found 433.2246.

*4.3.29. 2-(2-(2-(benzylamino)ethyl)-1H-benzo[d]imidazole-1-yl)-N-(2,3-dihydro-1H-indene-5-yl)acetamide **(36)***

Brown amorphous solid, yield: 70 mg (71%); m.p. 100–104 °C. ^{1}H NMR (MeOD, 400 MHz): δ = 1.96–2.03 (m, 2H, $CH_2C\underline{H}_2CH_2$), 2.77–2.81 (m, 4H, 2 × Ph-C$\underline{H}_2CH_2$), 3.10 (s, 4H, NH–C$\underline{H}_2$–C$\underline{H}_2$-Ar), 3.78 (s, 2H, Ph-C$\underline{H}_2$-NH), 5.03 (s, 1H, N–C$\underline{H}_2$–CO), 7.07–7.09 (m, 2H, 2 × Ar–$\underline{H}$), 7.17–7.28 (m, 7H, 7 × Ar–$\underline{H}$), 7.35–7.37 (m, 2H, 2 × Ar–$\underline{H}$), 7.55–7.57 (m, 1H, Ar–$\underline{H}$) ppm. ^{13}C NMR (MeOD, 100 MHz): δ = 26.70, 33.26, 33.92, 47.30, 54.10, 110.72, 117.54, 119.29, 119.49, 123.63, 124.01, 125.42, 128.44, 129.58, 129.67, 136.66, 137.36, 139.78, 141.71, 142.96, 146.11, 155.51, 167.01 ppm. MS (ESI): *m/z* (%) = 423.2 (M-H)$^-$. HPLC (254 nm): 94.7%, t_R = 8.46 min. HRMS Calcd for $C_{27}H_{27}N_4O$ *m/z*: 423.2185 (M-H)$^-$, found 423.2181.

4.3.30. N-(2,3-dihydro-1H-indene-5-yl)-2-(2-(2-((pyridine-4-ylmethyl)amino)ethyl)-1H-benzo[d]imidazole-1-yl)acetamide ***(37)***

Light brown amorphous solid, yield: 36 mg (59%); m.p. 93–97 °C. ^{1}H NMR (MeOD, 400 MHz): δ = 1.95–2.03 (m, 2H, $CH_2C\underline{H}_2CH_2$), 2.77–2.80 (m, 4H, 2 × Ph-C$\underline{H}_2$CH$_2$), 3.08 (s, 4H, NH–C$\underline{H}_2$–C$\underline{H}_2$-Ar), 3.79 (s, 2H, Py-C$\underline{H}_2$-NH), 5.06 (s, 1H, N–C$\underline{H}_2$–CO), 7.06–7.08 (m, 1H, Ar–$\underline{H}$), 7.15–7.22 (m, 3H, 3 × Ar–$\underline{H}$), 7.30–7.37 (m, 4H, 4 × Ar–$\underline{H}$), 7.54–7.57 (m, 1H, Ar–$\underline{H}$), 8.31–8.33 (m, 2H, 2 × Ar–$\underline{H}$) ppm. ^{13}C NMR (MeOD, 100 MHz): δ = 26.70, 28.17, 33.26, 33.92, 47.34, 47.91, 52.88, 110.75, 117.50, 119.25, 119.44, 123.62, 123.97, 124.87, 125.43, 136.68, 137.40, 141.69, 142.97, 146.12, 149.95, 151.63, 155.80, 167.03 ppm. MS (ESI): *m/z* (%) = 424.2 (M-H)$^-$. HPLC (254 nm): 93.2%, t_R = 3.46 min. HRMS Calcd for $C_{26}H_{26}N_5O$ *m/z*: 424.2137 (M-H)$^-$, found 424.2131.

4.3.31. N-(2,3-dihydro-1H-inden-5-yl)-2-(2-(2-(N-methylphenylsulfonamido)ethyl)-1H-benzo[d]imidazol-1-yl)acetamide ***(38)***

Brown amorphous solid. ^{1}H NMR (DMSO-d_6, 400 MHz): δ = 1.99 (p, 2H, *J* = 7.6 Hz, $CH_2C\underline{H}_2CH_2$), 2.79–2.83 (m, 7H, 2 × Ph-C$\underline{H}_2$-CH$_2$, C$\underline{H}_3$–N), 3.13 (t, 2H, *J* = 8.0 Hz, Ar-C$\underline{H}_2$-CH$_2$), 3.48 (t, 2H, *J* = 8.0 Hz, N–C$\underline{H}_2$–CH$_2$), 5.10 (s, 2H, N–C$\underline{H}_2$–CO), 7.15–7.22 (m, 3H, 3 × Ar–$\underline{H}$), 7.29 (d, 1H, *J* = 7.6 Hz, Ar–$\underline{H}$), 7.47 (d, 1H, *J* = 8.4 Hz, Ar–$\underline{H}$), 7.50 (s, 1H, Ar–$\underline{H}$), 7.57–7.62 (m, 3H, 3xAr-$\underline{H}$), 7.67–7.71 (m, 1H, Ar–$\underline{H}$), 7.78 (d, 2H, *J* = 7.2 Hz, 2 × Ar–$\underline{H}$), 10.41 (s, 1H, CO–N$\underline{H}$-Ar) ppm. ^{13}C NMR (DMSO-d_6, 100 MHz): δ = 25.62, 26.54, 32.25, 32.95, 35.73, 46.56, 48.20, 110.20, 115.96, 117.88, 118.97, 121.96, 122.39, 124.77, 127.53, 129.94, 133.47, 136.05, 137.19, 137.42, 139.42, 142.56, 144.77, 153.32, 165.60 ppm. HPLC (254 nm): 95.5%, t_R = 5.63 min. HRMS Calcd for $C_{27}H_{28}N_4O_3S$ *m/z*: 489.1955 (M-H)$^-$, found 489.1955.

4.3.32. N-(2,3-dihydro-1H-inden-5-yl)-2-(2-(2-((5-(dimethylamino)-N-methylnaphthalene)-1-sulfonamido)ethyl)-1H-benzo[d]imidazol-1-yl)acetamide ***(39)***

Brown amorphous solid. ^{1}H NMR (DMSO-d_6, 400 MHz): δ = 1.99 (t, 2H, *J* = 7.6 Hz, $CH_2C\underline{H}_2CH_2$), 2.73–2.89 (m, 10H, 2 × Ph-C$\underline{H}_2$-CH$_2$, (C$\underline{H}_3$)$_2$–N), 2,94 (s, 3H, C$\underline{H}_3$–N), 3.17 (t, 2H, *J* = 7.2 Hz, Ar-C$\underline{H}_2$-CH$_2$), 3.74 (t, 2H, *J* = 7.2 Hz, N–C$\underline{H}_2$–CH$_2$), 5.08 (s, 2H, N–C$\underline{H}_2$–CO), 7.14–7.29 (m, 5H, 5 × Ar–$\underline{H}$), 7.44–7.63 (m, 5H, 5 × Ar–$\underline{H}$), 8.09 (d, 1H, *J* = 6.8 Hz, Ar–$\underline{H}$), 8.19 (d, 1H, *J* = 8.4 Hz, Ar–$\underline{H}$), 8.48 (d, 1H, *J* = 8.4 Hz, Ar–$\underline{H}$), 10.39 (s, 1H, CO–N$\underline{H}$-Ar) ppm. ^{13}C NMR (DMSO-d_6, 100 MHz): δ = 26.62, 26.44, 32.25, 32.94, 35.09, 45.51, 46.56, 47.74, 110.17, 115.71, 116.00, 117.91, 118.97, 119.36, 121.97, 122.40, 124.16, 124.76, 128.59, 129.10, 129.73, 129.88, 130.35, 134.75, 136.01, 137.16, 139.43, 142.56, 144.76, 151.87, 153.32, 165.57 ppm. HPLC (254 nm): 95.1%, t_R = 5.52 min. HRMS Calcd for $C_{33}H_{35}N_5O_3S$ *m/z*: 582.2533 (M-H)$^-$, found 582.2524.

4.3.33. N-(2,3-dihydro-1H-inden-5-yl)-2-(2-(3-(phenylsulfonamido)propyl)-1H-benzo[d]imidazol-1-yl)acetamide ***(41)***

Brown amorphous solid. ^{1}H NMR (DMSO-d_6, 400 MHz): δ = 1.91–2.03 (m, 4H, 2 × $CH_2C\underline{H}_2CH_2$), 2.78–2.83 (m, 6H, 2 × Ph-C$\underline{H}_2$-CH$_2$, Ar-C$\underline{H}_2$-CH$_2$), 2.91 (q, 2H, *J* = 6.4 Hz, CH$_2$–C$\underline{H}_2$–NH), 5.03 (s, 2H, N–C$\underline{H}_2$–CO), 7.13–7.19 (m, 3H, 2 × Ar–$\underline{H}$, CH$_2$–N$\underline{H}$–SO$_2$), 7.29 (d, 1H, *J* = 8.0 Hz, Ar–$\underline{H}$), 7.43 (d, 1H, *J* = 6.4 Hz, Ar–$\underline{H}$), 7.50 (s, 1H, Ar–$\underline{H}$), 7.55–7.64 (m, 4H, 4 × Ar–$\underline{H}$), 7.74 (t, 1H, *J* = 6.0 Hz, Ar–$\underline{H}$), 7.79 (d, 2H, *J* = 6.8 Hz, 2 × Ar–$\underline{H}$), 10.38 (s, 1H, CO–N$\underline{H}$-Ar) ppm. ^{13}C NMR (DMSO-d_6, 100 MHz): δ = 24.10, 25.62, 27.02, 32.25, 32.94, 42.71, 46.46, 110.05, 115.96, 117.87, 118.83, 121.79, 122.13, 124.76, 126.93, 129.66, 132.81, 136.31, 137.19, 139.40, 140.85, 142.60, 144.77, 155.57, 165.59 ppm. HPLC (254 nm): 98.1%, t_R = 5.47 min. HRMS Calcd for $C_{27}H_{28}N_4O_3S$ *m/z*: 489.1955 (M-H)$^-$, found 489.1948.

4.3.34. N-(2,3-dihydro-1H-inden-5-yl)-2-(2-(3-(N-methylphenylsulfonamido)propyl)-1H-benzo[d]imidazol-1-yl)acetamide ***(42)***

Brown amorphous solid. ^{1}H NMR (DMSO-d_6, 400 MHz): δ = 1.98–2.06 (m, 4H, 2 × $CH_2C\underline{H}_2CH_2$), 2,69 (s, 3H, C$\underline{H}_3$–N), 2.74–2.89 (m, 6H, 2 × Ph-C$\underline{H}_2$-CH$_2$, Ar-C$\underline{H}_2$-CH$_2$), 3.10 (t, 2H, *J* = 6.8 Hz, CH$_2$–C$\underline{H}_2$–NH), 5.08 (s, 2H, N–C$\underline{H}_2$–CO), 7.17 (br s, 3H, 3 × Ar–$\underline{H}$), 7.30 (d, 1H, *J* = 7.6 Hz, Ar–$\underline{H}$), 7.46 (d, 1H, *J* = 7.2 Hz, Ar–$\underline{H}$), 7.51 (s, 1H, Ar–$\underline{H}$), 7.57–7.63 (m, 3H, 3 × Ar–$\underline{H}$), 7.67–7.70 (m, 1H, Ar–$\underline{H}$), 7.77 (d, 2H, *J* = 7.2 Hz, 2 × Ar–$\underline{H}$), 10.40 (s, 1H, CO–N$\underline{H}$-Ar) ppm. ^{13}C NMR (DMSO-d_6, 100 MHz): δ = 23.99, 25.15, 25.62, 32.25, 32.94, 35.10, 46.52, 49.78, 110.09, 115.97, 117.88, 118.86, 121.79, 122.13, 124.77, 127.61, 129.87, 133.39, 136.21, 137.20, 137.25, 139.41, 142.65, 144.78, 155.55, 165.66 ppm. HPLC (254 nm): 95.0%, t_R = 5.77 min. HRMS Calcd for $C_{28}H_{30}N_4O_3S$ *m/z*: 503.2111 (M-H)$^-$, found 503.2101.

4.4. Cell culture

4.4.1. HEK-blue NOD1 and NOD2 cells

HEK-Blue NOD1 and NOD2 cells (Invivogen) were cultured in DMEM medium (Sigma-Aldrich, St. Louis/MO, USA) with 10% heat-deactivated FBS (Gibco), 2 mM L-glutamine (Sigma-Aldrich, St. Louis/MO, USA), 50 U/mL penicillin (Sigma-Aldrich, St. Louis/MO, USA), 50 ng/mL streptomycin (Sigma-Aldrich, St. Louis/MO, USA), 4.5 g glucose (Sigma-Aldrich, St. Louis/MO, USA) and 100 μg/mL Normocin (Invivogen) for 2 passages. All subsequent passages were cultured in the medium supplemented with 30 μg/mL blasticidin (Invivogen) and 100 μg/mL zeocin (Invivogen). The experiments were carried out on passages 7–12.

4.4.2. THP-1 cells

For all experiments, THP-1 cells (Istituto Zooprofilattico di Brescia, Brescia, Italy) were diluted to 10^6 cells/mL in RPMI 1640 containing 2 mM L-glutamine, 0.1 mg/mL streptomycin, 100 IU/mL penicillin, 50 μM 2-mercaptoethanol, supplemented with 10% heat-inactivated foetal calf serum (media) and cultured at 37 °C in 5% CO_2. The experiments were carried out on passages 3–12. To evaluate IL-8 and TNF-α production, cultures were set up in 24-well culture plates containing 500 μL of cells. They were pre-treated with selected NOD antagonists at 20 μM for 1 h before the addition of either MDP or C12-iE-DAP (both at 10 μM) and then incubated for 20 h. Each concentration was tested in triplicate, untreated cells were exposed to DMSO which represented the vehicle control (0.2% final concentration was not exceeded). In synergy studies, cells were additionally stimulated with lipopolysaccharide (LPS, from *Escherichia coli* serotype 0127:B8, Sigma) at a final concentration of 1 ng/mL as indicated in the figure legends. Cell-free supernatants were collected at 18 h and stored at −80 °C before being evaluated for cytokines by a commercially available kit.

4.4.3. PBMCs

Human PBMC from healthy blood donors were isolated by density gradient centrifugation with Ficoll-Paque (Pharmacia, Sweden). The cells were cultured in RPMI 1640 (Sigma, Germany) supplemented with 100 U/mL penicillin (Sigma-Aldrich, St. Louis/MO, USA), 100 μg/mL streptomycin (Sigma-Aldrich, St. Louis/MO, USA), 2 mM L-glutamine (Sigma-Aldrich, St. Louis/MO, USA), 50 μM 2-mercaptoethanol (Sigma-Aldrich, St. Louis/MO, USA) and 10% heat-inactivated foetal bovine serum (Gibco, USA). 1 × 10^6 cells were plated on 24-well culture plates (Nunc, Denmark) and cultivated at 37 °C in a humidified atmosphere of 5% CO_2 in air.

4.5. Metabolic activity/cell viability assay

The tested compounds were dissolved in DMSO and further diluted in culture medium to a desired final concentration, so that the final concentration of DMSO did not exceed 0.1%. HEK-Blue NOD1 cells (1×10^4 cells/well) were seeded in triplicates on 96 well plates in 100 μL culture medium and treated with 20 μM concentration of each compound or with the corresponding volume of vehicle – 0.1% DMSO (control cells). After 18 h, metabolic activity was measured using the CellTiter 96® Aqueous One Solution Cell Proliferation Assay (Promega, Madison/WI, USA), in accordance with the manufacturer's instructions. Three biological replicates were performed for each experiment.

Prior to investigating the effects of selected NOD antagonists on cytokine production, their potential cytotoxicity for THP-1 cells was assessed. Cell viability was assessed by leakage of lactate dehydrogenase from damaged cells. Cells were treated for 18 h with the compound of interest at concentrations of up to 20 μM. LDH activity was determined in cell-free supernatants using a commercially available colorimetric kit (Takara Bio Inc., Kusatsu, Japan). Results are expressed as OD.

4.6. Measurement of NF-κB transcriptional activity (HEK-Blue detection)

For screening for potential NOD antagonists, HEK-Blue NOD2 and NOD1 cells (5×10^5 cells/mL) were assayed in duplicate for NF-κB transcriptional activity after treatment with 10 μM compounds for 1 h, followed by the addition of 2 μM MDP or 100 nM C12-iE-DAP, respectively, and subsequent incubation for 18 h (37 °C, 5% CO_2, 100% humidity). The tested compounds were dissolved in DMSO and further diluted in culture medium to a desired final concentration, so that the final concentration of DMSO did not exceed 0.1%. The control cells (NT) were only treated with the corresponding volume of vehicle – 0.1% DMSO. For determining IC_{50}, HEK-Blue NOD2 and NOD1 cells (5×10^5 cells/mL) were assayed in duplicates for NF-κB transcriptional activity after 1 h pre-treatment with 0.3125–20 μM NOD antagonists or noditinib-1, followed by the addition of 2 μM MDP or 100 nM C12-iE-DAP, respectively, and subsequent incubation for 18 h. SEAP activity was determined spectrophotometrically as absorbance at 620 nm on a Tecan Safire 2 microplate reader (Reading, UK). Assays were performed in three biological replicates.

4.7. Cytokine production (ELISA)

IL-8 and TNF-α release from THP-1 cells were measured in cell-free supernatants obtained by centrifugation at 3000 rpm for 5 min and stored at −80 °C until measurement. IL-8 and TNF-α production were assessed by specific sandwich ELISA (Immunotools, Friesoythe, Germany; eBioScience or R&D System Minneapolis, MN, USA). Results are expressed in pg/ml. Limit of detection was 15.6 pg/mL for IL-8 and 4 pg/mL for TNF-α.

4.8. Multiplexed cytokine assays

PBMCs were treated with MDP (2 μM) in the presence or absence of 20 μM of compound **32**. Cell-free supernatants were collected at 18 h and stored at −80 °C before being evaluated for cytokines by a commercially available kit. Cytokine production was assessed by BD Cytometric Bead Array Human Th1/Th2 Kit (Content: IL-2, IL-4, IL-6, IL-10, TNF-α, IFNγ). Flow cytometric analyses were performed using a FACSCalibur flow cytometer with Sorting Option: 4-Color and CELLQuest software (BD Biosciences; San Diego, CA, USA). Standard curves were generated using recombinant cytokines provided in the kit. The data were analyzed with FlowJo software (Tree Star, Inc., Ashland, OR). Results are expressed in pg/mL. Data are means ± standard deviation from two representative independent experiments.

4.9. Statistics

All experiments were performed at least twice, with average values expressed as means ± SD. IC_{50} values of NOD1/2 inhibition were calculated by a non-linear regression model using Graph Pad Prism 6 software (La Jolla, CA, USA). Statistical significance was determined with the Dunnet multiple comparison test as indicated in the figure legends. Differences were considered nonsignificant for $p > 0.05$, significant (*) for $p < 0.05$, very significant (**) for $p < 0.01$ and extremely significant (***) for $p < 0.001$.

Declaration of competing interest

The authors declare that they have no known competing financial interests or personal relationships that could have appeared to influence the work reported in this paper.

Acknowledgments

This research was funded by the Slovenian Research Agency (Grant No. P1-0208) and COST action CA15135 "Multi-target paradigm for innovative ligand identification in the drug discovery process (MuTaLig)" (Grant ID STSM-CA15135-090117-082301). The authors thank dr. Chris Berrie for proofreading the manuscript.

Appendix A. Supplementary data

Supplementary data to this article can be found online at https://doi.org/10.1016/j.ejmech.2020.112089.

References

[1] J.H. Fritz, R.L. Ferrero, D.J. Philpott, et al., Nod-like proteins in immunity, inflammation and disease, Nat. Immunol. 7 (2006) 1250–1257.
[2] R. Caruso, N. Warner, N. Inohara, G. Nuñez, NOD1 and NOD2: signaling, host defense, and inflammatory disease, Immunity 41 (2014) 898–908.
[3] D.J. Philpott, M.T. Sorbara, S.J. Robertson, K. Croitoru, S.E. Girardin, NOD proteins: regulators of inflammation in health and disease, Nat. Rev. Immunol. 14 (2014) 9–23.
[4] S. Nabergoj, I. Mlinarič-Raščan, Ž. Jakopin, Harnessing the untapped potential of nucleotide-binding oligomerization domain ligands for cancer immunotherapy, Med. Res. Rev. 39 (2019) 1447–1484.
[5] S.E. Girardin, I.G. Boneca, L.A.M. Carneiro, A. Antignac, M. Jéhanno, J. Viala, K. Tedin, M.K. Taha, A. Labigne, U. Zähringer, A.J. Coyle, P.S. DiStefano, J. Bertin, P.J. Sansonetti, D.J. Philpott, Nod1 detects a unique muropeptide from gram-negative bacterial peptidoglycan, Science 300 (2003) 1584–1587.
[6] S.E. Girardin, M. Jéhanno, D. Mengin-Lecreulx, P.J. Sansonetti, P.M. Alzari, D.J. Philpott, Identification of the critical residues involved in peptidoglycan detection by Nod1, J. Biol. Chem. 280 (2005) 38648–38656.
[7] M. Chamaillard, M. Hashimoto, Y. Horie, J. Masumoto, S. Qiu, L. Saab, Y. Ogura, A. Kawasaki, K. Fukase, S. Kusumoto, M.A. Valvano, S.J. Foster, T.W. Mak, G. Nuñez, N. Inohara, An essential role for NOD1 in host recognition of bacterial peptidoglycan containing diaminopimelic acid, Nat. Immunol. 4 (2003) 702–707.
[8] S.E. Girardin, L.H. Travassos, M. Hervé, D. Blanot, I.G. Boneca, D.J. Philpott, P.J. Sansonetti, D. Mengin-Lecreulx, Peptidoglycan molecular requirements allowing detection by Nod1 and Nod2, J. Biol. Chem. 278 (2003) 41702–41708.
[9] N. Inohara, Y. Ogura, A. Fontalba, O. Gutierrez, F. Pons, J. Crespo, K. Fukase, S. Inamura, S. Kusumoto, M. Hashimoto, S.J. Foster, A.P. Moran, J.L. Fernandez-Luna, G. Nuñez, Host recognition of bacterial muramyl dipeptide mediated through NOD2, J. Biol. Chem. 278 (2003) 5509–5512.
[10] Ž. Jakopin, Nucleotide-binding oligomerization domain (NOD) inhibitors: a rational approach toward inhibition of NOD signaling pathway, J. Med. Chem. 57 (2014) 6897–6918.
[11] R.G. Correa, S. Milutinovic, J.C. Reed, Roles of NOD1 (NLRC1) and NOD2 (NLRC2) in innate immunity and inflammatory diseases, Biosci. Rep. 608 (2012) 597–608.
[12] L.O. Moreira, D.S. Zamboni, NOD1 and NOD2 signaling in infection and inflammation, Front. Immunol. 3 (2012) 328.
[13] L. Moreno, T. Gatheral, Therapeutic targeting of NOD1 receptors, Br. J. Pharmacol. 170 (2013) 475–485.
[14] S. Wang, J. Yang, X. Li, et al., Discovery of 1,4-Benzodiazepine-2,5-dione (BZD) derivatives as dual nucleotide binding oligomerization domain containing 1/

2 (NOD1/NOD2) antagonists sensitizing paclitaxel (PTX) to suppress lewis lung carcinoma (LLC) growth in vivo, J. Med. Chem. 60 (2017) 5162–5192.
[15] G. Magnuson, P. Khan, H. Yuan, B. Brown, D.B. Divlianska, D. Stonich, S. Peddibhotla, Y. Su, S. Dad, E. Sergienko, T.D.Y. Chung, G.P. Roth, C. Wimer, P. Diaz, R.G. Correa, J.C. Reed, High Throughput Screening Assays for NOD1 Inhibitors – Probe 1. Probe Reports from the NIH Molecular Libraries Program, 2010 Bethesda (MD).
[16] G. Magnuson, P. Khan, H. Yuan, B. Brown, D.B. Divlianska, D. Stonich, S. Peddibhotla, Y. Su, S. Dad, E. Sergienko, T.D.Y. Chung, G.P. Roth, C. Wimer, P. Diaz, R.G. Correa, J.C. Reed, High Throughput Screening Assays for NOD1 Inhibitors – Probe 2. Probe Reports from the NIH Molecular Libraries Program, 2010 Bethesda (MD).
[17] D.J. Rickard, C.A. Sehon, V. Kasparcova, L.A. Kallal, P.A. Haile, X. Zeng, M.N. Montoute, D.D. Poore, H. Li, Z. Wu, P.M. Eidam, J.G. Emery, R.W. Marquis, P.J. Gough, J. Bertin, Identification of selective small molecule inhibitors of the nucelotide-binding oligomerization domain 1 (NOD1) signaling pathway, PloS One 9 (2014) e96737.
[18] P.M. Khan, R.G. Correa, D.B. Divlianska, S. Peddibhotla, E.H. Sessions, G. Magnuson, B. Brown, E. Suyama, H. Yuan, A. Mangravita-Novo, M. Vicchiarelli, Y. Su, S. Vasile, L.H. Smith, P.W. Diaz, J.C. Reed, G.P. Roth, Identification of inhibitors of NOD1-induced nuclear factor-κB activation, ACS Med. Chem. Lett. 2 (2011) 780–785.
[19] R.G. Correa, P.M. Khan, N. Askari, D. Zhai, M. Gerlic, B. Brown, G. Magnuson, R. Spreafico, S. Albani, E. Sergienko, P.W. Diaz, G.P. Roth, J.C. Reed, Discovery and characterization of 2-aminobenzimidazole derivatives as selective NOD1 inhibitors, Chem. Biol. 18 (2011) 825–832.
[20] D.J. Rickard, C.A. Sehon, V. Kasparcova, et al., Identification of benzimidazole diamides as selective inhibitors of the nucleotide-binding oligomerization domain 2 (NOD2) signaling pathway, PloS One 8 (2013) e69619.
[21] K. Keček Plešec, D. Urbančič, M. Gobec, et al., Identification of indole scaffold-based dual inhibitors of NOD1 and NOD2, Bioorg. Med. Chem. 24 (2016) 5221–5234.
[22] Ž. Jakopin, E. Corsini, M. Gobec, I. Mlinarič-Raščan, M. Sollner Dolenc, Design, synthesis and biological evaluation of novel desmuramyldipeptide analogs, Eur. J. Med. Chem. 46 (2011) 3762–3777.
[23] Ž. Jakopin, M. Gobec, I. Mlinarič-Raščan, M. Sollner Dolenc, Immunomodulatory properties of novel nucleotide oligomerization domain 2 (Nod2) agonistic desmuramyldipeptides, J. Med. Chem. 55 (2012) 6478–6488.
[24] Ž. Jakopin, The design and synthesis of Ala-Glu/iGln mimetics: heterocyclic building blocks for pseudopeptides, Tetrahedron Lett. 56 (2015) 504–506.
[25] Ž. Jakopin, Murabutide revisited: a review of its pleiotropic biological effects, Curr. Med. Chem. 20 (2013) 2068–2079.
[26] M. Gobec, I. Mlinarič-Raščan, M. Sollner Dolenc, Ž. Jakopin, Structural requirements of acylated Gly-l-Ala-d-Glu analogs for activation of the innate immune receptor NOD2, Eur. J. Med. Chem. 116 (2016) 1–12.
[27] M. Gobec, T. Tomašič, A. Štimac, et al., Discovery of nanomolar desmuramylpeptide agonists of the innate immune receptor nucleotide-binding oligomerization domain-containing protein 2 (NOD2) possessing immunostimulatory properties, J. Med. Chem. 61 (2018) 2707–2724.
[28] Ž. Jakopin, M. Gobec, J. Kodela, T. Hazdovac, I. Mlinarič-Raščan, M. Sollner Dolenc, Synthesis of conformationally constrained γ-D-glutamyl-meso-diaminopimelic acid derivatives as ligands of nucleotide-binding oligomerization domain protein 1 (Nod1), Eur. J. Med. Chem. 69 (2013) 232–243.
[29] J. Mo, J.P. Boyle, C.B. Howard, T.P. Monie, B.K. Davis, J.A. Duncan, Pathogen sensing by nucleotide-binding oligomerization domain-containing protein 2 (NOD2) is mediated by direct binding to muramyl dipeptide and ATP, J. Biol. Chem. 287 (2012) 23057–23067.
[30] B. Zurek, H. Bielig, T.A. Kufer, Cell-based reporter assay to analyze activation of Nod1 and Nod2, Methods Mol. Biol. 748 (2011) 107–119.
[31] Ž. Jakopin, E. Corsini, THP-1 cells and pro-inflammatory cytokine production: an *in vitro* tool for functional characterization of NOD1/NOD2 antagonists, Int. J. Mol. Sci. 20 (2019) pii: E4265, doi:10.3390/ijms20174265.
[32] A.F. Abdel-Magid, K.G. Carson, B.D. Harris, C.A. Maryanoff, R.D. Shah, Reductive amination of aldehydes and ketones with sodium triacetoxyborohydride. Studies on direct and indirect reductive amination procedures, J. Org. Chem. 61 (1996) 3849–3862.
[33] M. Živec, Ž. Jakopin, S. Gobec, Recent advances in the synthesis and applications of reduced amide pseudopeptides, Curr. Med. Chem. 16 (2009) 2289–2304.
[34] A. Uehara, S. Yang, Y. Fujimoto, et al., Muramyldipeptide and diaminopimelic acid-containing desmuramylpeptides in combination with chemically synthesized toll-like receptor agonists synergistically induced production of interleukin-8 in a NOD2- and NOD1-dependent manner, respectively, in human monocytic cells in culture, Cell Microbiol. 7 (2005) 53–61.
[35] L. Zhao, M.J. Kwon, S. Huang, et al., Differential modulation of nods signaling pathways by fatty acids in human colonic epithelial HCT116 cells, J. Biol. Chem. 283 (2007) 11618–11628.
[36] J. da Silva Correia, Y. Miranda, N. Austin-Brown, et al., Nod1-Dependent control of tumor growth, Proc. Natl. Acad. Sci. U.S.A. 103 (2006) 1840–1845.
[37] J.H. Fritz, S.E. Girardin, C. Fitting, et al., Synergistic stimulation of human monocytes and dendritic cells by toll-like receptor 4 and Nod1- and nod2-activating agonists, Eur. J. Immunol. 35 (2005) 2459–2470.
[38] J. Uehori, K. Fukase, T. Akazawa, et al., Dendritic cell maturation induced by muramy dipeptide (MDP) derivatives: monoacylated MDP confers TLR2/TLR4 activation, J. Immunol. 174 (2005) 7096–7103.
[39] H. Tada, S. Aiba, K. Shibata, et al., Synergistic effect of Nod1 and Nod2 agonists with toll-like receptor agonists on human dendritic cells to generate interleukin-12 and T helper type 1 cells, Infect. Immun. 73 (2005) 7967–7976.
[40] A.I. Tukhvatulin, A.S. Dzharullaeva, N.M. Tukhvatulina, et al., Powerful complex immunoadjuvant based on synergistic effect of combined TLR4 and NOD2 activation significantly enhances magnitude of humoral and cellular adaptive immune responses, PloS One 11 (2016) e0155650.
[41] D.A. van Heel, S. Ghosh, M. Butler, et al., Synergistic enhancement of toll-like receptor responses by NOD1 activation, Eur. J. Immunol. 35 (2005) 2471–2476.
[42] C.R. Kleiveland, Chapter 15 Peripheral blood mononuclear cells, in: K. Verhoeckx (Ed.), The Impact of Food Bioactives on Health: In Vitro and Ex Vivo Models, Springer, Cham (CH), 2015, pp. 161–167.
[43] J.F. Viallard, J.L. Pellegrin, V. Ranchin, T. Schaeverbeke, J. Dehais, M. Longy-Boursier, J.M. Ragnaud, B. Leng, J.F. Moreau, Th1 (IL-2, interferon-gamma (IFN-γ)) and Th2 (IL-10, IL-4) cytokine production by peripheral blood mononuclear cells (PBMC) from patients with systemic lupus erythematosus (SLE), Clin. Exp. Immunol. 115 (1999) 189–195.